

## **Myres Hill study:**

A comparison between the Heriot-Watt wind farm model and LIDAR data

7<sup>th</sup> July 2009

Dr Angus C.W. Creech  
School of Engineering and Physical Sciences  
Heriot-Watt University  
Scotland  
EH14 4AS

**Email:** [acwc2@hw.ac.uk](mailto:acwc2@hw.ac.uk)

# Contents

1	Foreword	4
2	Methodology	5
2.1	Site and turbine selection	5
2.2	Hardware and software upgrade	6
2.3	Importing topography	6
2.3.1	GMSH	7
2.3.2	GMT tools	7
2.3.3	Mesh warping	8
2.4	Ground features	8
2.5	Wind profiles	9
	Note	10
2.6	Turbine model configuration	10
2.6.1	Main specifications	10
2.6.2	Blade geometry	11
2.6.3	Lift and drag characteristics	12
2.6.4	Turbine control mechanisms	13
3	Results from simulation and experiment	15
3.1	Notes on modelling	15
3.1.1	Simulation run times	15
3.1.2	Extrapolation of boundary conditions	15
3.2	Flow within the model turbine	15
3.3	Power output and torque	17
3.4	Wake results	18
3.4.1	The LIDAR wake data	18
3.4.2	The turbine model wake data	20
3.4.3	Comparison of wake profiles	22
3.5	Model flow visualisation	23
3.5.1	Horizontal slice	23
3.5.2	Vertical slice	29
3.5.3	Mesh evolution	35
4	Discussion	38
4.1	Qualitative assessment	38
4.1.1	Turbine performance	38

4.1.2	Flow modelling over terrain	38
4.1.3	Wake modelling	39
4.2	Future work	39
5	Conclusion	41

# 1 Foreword

Commercial wind farm modelling software such as WindFarmer, WindSim and WAsP all use semi-analytical models in predicting wind turbine wakes. Recent research by one of the original authors of WAsP<sup>1</sup> suggests that a computational fluid dynamics (CFD) approach could provide more accurate prediction of wind turbine performance. However, this approach does have its difficulties – primarily that of computational complexity.

At Heriot-Watt, a wind and marine turbine model has been developed that adopts a full CFD approach for wake modelling. This is capable of simulating the unsteady, turbulent flow in turbines and their wakes over relatively large domains, whilst also predicting the performance of multiple turbines. This has been tested and verified in idealised domains<sup>2</sup>. Recently, portions of blade element momentum (BEM) have been incorporated into the model, allowing blade geometry and lift/drag characteristics from real-life turbines to be fed in as parameters.

The next step in validation of this model, prior to any commercial use, is to simulate a real wind turbine, situated in a domain with topography, ground features, and complex flow conditions – and validate it with results from wind measurements around the real turbine. In this regard, LIDAR presents the most promising prospect for detailed wake measurement, and with it, model validation.

SgurrEnergy Ltd. have developed a LIDAR device called Galion, which is capable of three-dimensional measurements of air flow over long distances. This represents a unique opportunity to give the Heriot-Watt model a thorough validation, whilst developing the necessary methodology in the process.

This document details the work undertaken at Heriot Watt by Dr. Creech during a joint project with SgurrEnergy, in which the turbine model was tested against LIDAR data, and techniques developed so that it can easily be configured for simulation of real world sites and turbines.

---

<sup>1</sup> Rebecca Barthelmie et al. Power losses due to wakes in large wind farms. *World Renewable Energy Congress (WRECX) 2008*.

<sup>2</sup> Angus C.W. Creech. A three-dimensional numerical model of a horizontal axis, energy extracting turbine. PhD thesis. *Heriot-Watt University, 2008*.

## 2 Methodology

The Heriot-Watt turbine model uses an academic CFD package called Fluidity<sup>3</sup> to handle solution of the Navier-Stokes equations and the turbulence modelling through Large Eddy Simulation (LES) with Smagorinsky algorithms<sup>4</sup>. Whilst it is capable of simulating air flow over terrain, as research code it demands a highly technical approach to adapt terrain data, etc. for use with it – this often requires the end user to write additional software to extend Fluidity’s features. The beauty of this is that a great deal of flexibility is afforded in simulations, and that once methodologies and additional software is in place, newer simulations can be configured and run with much greater efficiency.

This section will detail the steps taken at Heriot Watt to prepare Fluidity for use in the simulation of wind turbines in realistic terrain.

### 2.1 Site and turbine selection

After some discussion with Sgurr, it was decided that the Myres Hill test facility near East Kilbride would be selected as the site for measuring wind turbine wakes. Whilst Myres Hill is owned and operated by TUV NEL, Sgurr have access to the site and have tested the Galion device there before.

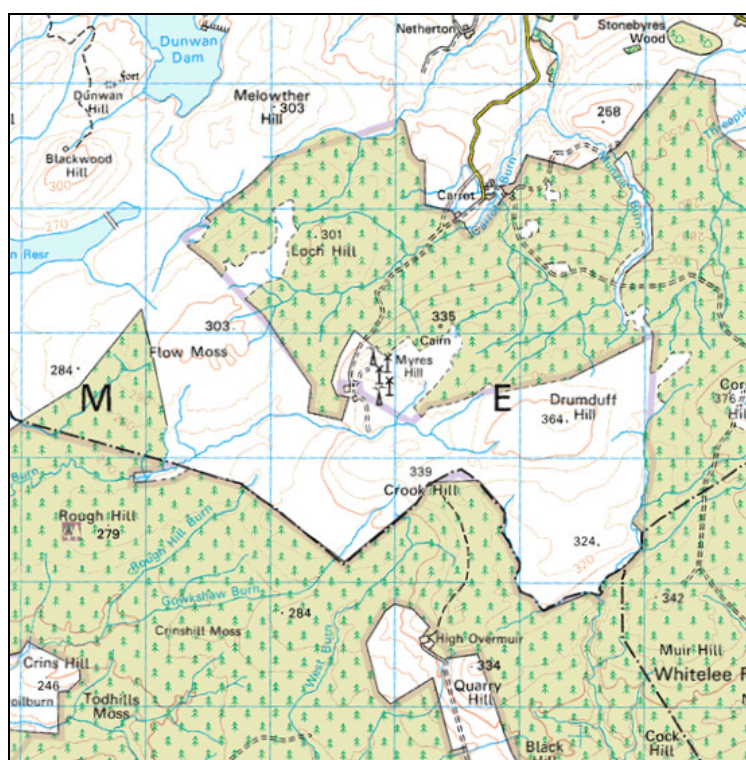


Figure 1: Ordnance Survey (OS) map of Myres Hill

<sup>3</sup> M.D. Piggott, C. Pain et al. *Fluidity/ICOM Manual*. Applied Modelling and Computation Group, Imperial College in London, England, 2007.

<sup>4</sup> M. Lesieur and O. Métais. New trends in large-eddy simulations of turbulence, *Annual Review of Fluid Mechanics* #28, 1996.

Previous Galion LIDAR measurements had been taken around one of the 950kW NEG Micon NM54 turbines (situated at the centre of Figure 1); this turbine would be the one selected for modelling. OS contour data at 10m intervals was provided over a 6km x 6km area, which would serve as the topography for the model domain.

## **2.2 Hardware and software upgrade**

Prior to the project, a 2 year old copy of Fluidity with the turbine model attached had been running on a 4GB dual-core, dual processor Opteron Linux system. For the scale of the simulations to be run, this was insufficient: a 8GB quad-core, dual processor Xeon Linux system was purchased. Fluidity was also upgraded to the latest version; this required familiarisation with a different framework and a different set of tools, namely:

- XML-based simulation configuration tool, Diamond.
- GMSH meshing utility – creates the finite element meshes used in Fluidity
- Installation of supporting software, ie. PETSc, ParMetis, Intel IFort v10.2, OpenMPI, etc.

It should be noted that installing of, and familiarisation with the upgraded version of Fluidity were rather protracted processes, as there is no user manual nor installation instructions at the time of writing.

## **2.3 Importing topography**

At this stage, contour data had to be imported into Fluidity. An early problem encountered was that the meshing program used with Fluidity, GMSH, cannot currently generate 3D dimensional, unstructured meshes with irregular boundaries, necessary for simulation of flow over terrain; it was designed to handle simpler, geometric shapes. Four steps were necessary for Fluidity and GMSH to work with irregular boundaries, as illustrated in Figure 2:

1. An initial cuboidal mesh that broadly represents the computation domain is generated using GMSH. An example can be seen in Figure 3.
2. The contour data is transformed into a regular grid of elevation data. The Generic Mapping Tools (GMT) software<sup>5</sup> are used to create this grid.
3. A bespoke utility warps this mesh, so that the lower surface follows the terrain.
4. A second program locks the lower surface, so that Fluidity preserves the shape of the terrain.

---

<sup>5</sup> The Generic Mapping Tools home page. Website. <http://gmt.soest.hawaii.edu/>.

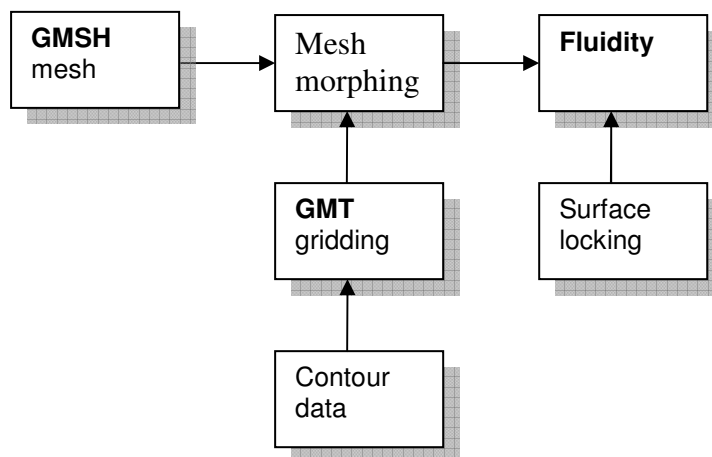


Figure 2: The process of importing contour data into Fluidity

### 2.3.1 GMSH

GMSH<sup>6</sup> is a freely available meshing program available on many Linux distributions, used to create the initial meshes. The domain covers the maximum extent of the contour map.

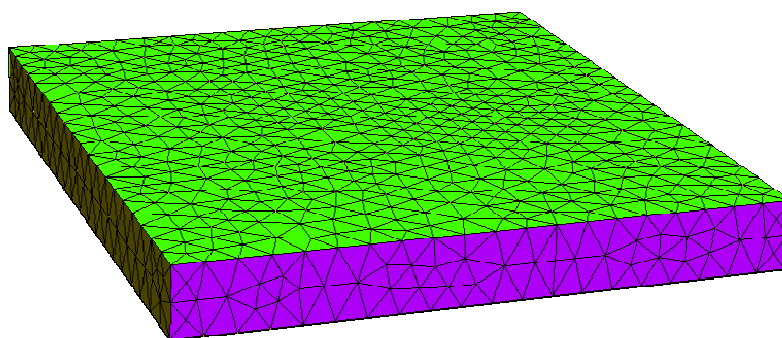


Figure 3: the initial GMSH mesh for Myres Hill

### 2.3.2 GMT tools

The Generic Mapping Tools are used to convert the contour map of Myres Hill, which is an irregular, sparse data set, into a regular gridded format which can then be easily processed. The interval in the grid spacing was set to 25m.

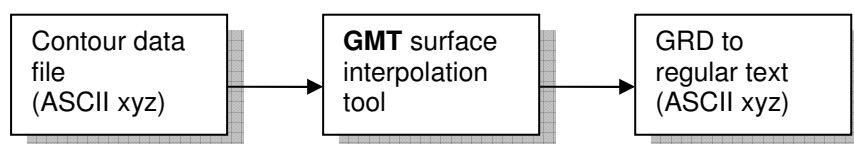


Figure 4: creation of regular gridded elevation file

The regular grid ASCII text file in Figure 4 is used by the mesh warping utility to distort the initial GMSH mesh to fit topographic data.

---

<sup>6</sup> GMSH home page. Website. <http://www.geuz.org/gmsh/>

### 2.3.3 Mesh warping

A utility written in Python parses the mesh file generated by GMSH, using data from the gridded elevation data file. It shrinks the range of the vertical components, so that the ceiling of the domain is preserved, whilst the bottom of the mesh is raised according to the topography as shown in Figure 5.

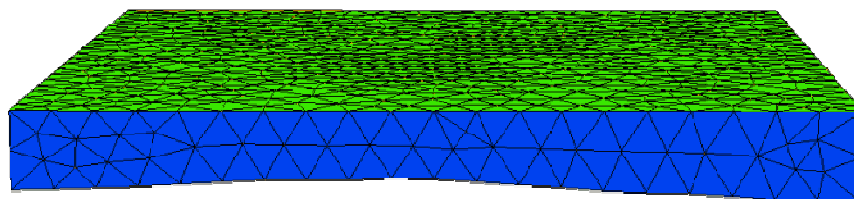


Figure 5: GMSH mesh warped to fit topography

A new mesh file is constructed and named *morphed-xxxx.msh*, where *xxxx* is the project name. It is this mesh file that is loaded into Fluidity.

## 2.4 Ground features

To account for the effect on air flow by different ground features such as trees and grass, a roughness map had to be generated. An OS map of the area, left in

Figure 6, was transformed with a graphics package into an indexed greyscale image, as seen on the right, and saved in portable graymap (PGM) format.

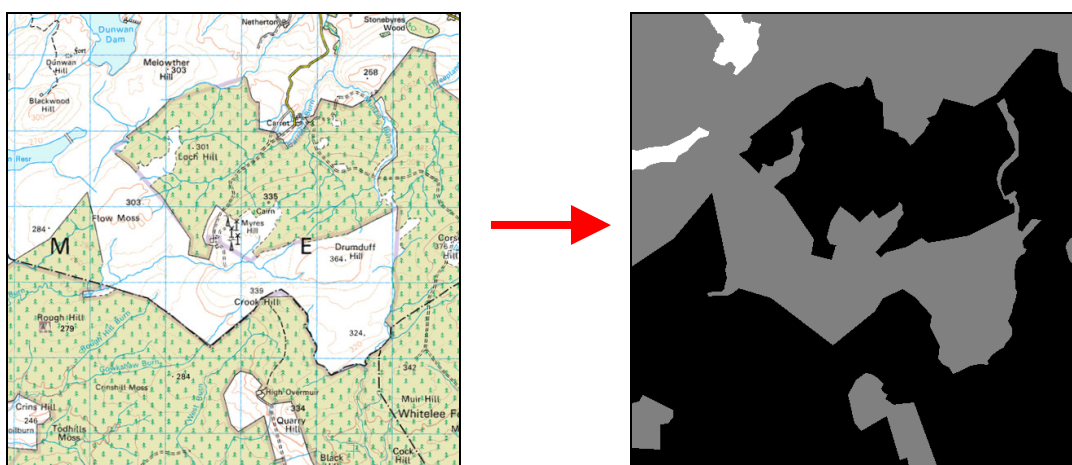


Figure 6: transition from OS map to identified ground features. The black shading represents trees, the grey shading rough grass/heather, and white is water.

This PGM format image file was then parsed by a Python utility into a series of spatially-varying drag coefficients, roughness lengths and feature height (used to calculate zero-plane displacement), taken from WASP documentation and atmospheric science journal papers<sup>7 8</sup> and listed in Table 1. This was saved to a separate file in a variation of the ASCII xyz format.

<sup>7</sup> A. Cescatti and B. Marcolla. Drag Coefficient and turbulence intensity in conifer canopies. *Agricultural and Forest Meteorology* #121, 2004.

Ground feature	Drag coefficient	Roughness length (m)	Feature height(m)
Forestry	0.3	1.0	30.0
Grass or heather	0.005	0.03	0.5
Water	0.00001	0.0002	0.01

Table 1: ground feature values for drag coefficient, roughness length and feature height

## 2.5 Wind profiles

The mean wind speed in the boundary layer of the atmosphere can be approximated as a logarithmic wind profile (see Figure 7 for examples). This was assumed to be the case at the sides of the simulation domain, with no flow in the vertical direction; the wind direction can be specified arbitrarily. These profiles were imposed as weak Dirichlet boundary conditions, so as to not violate continuity of mass.

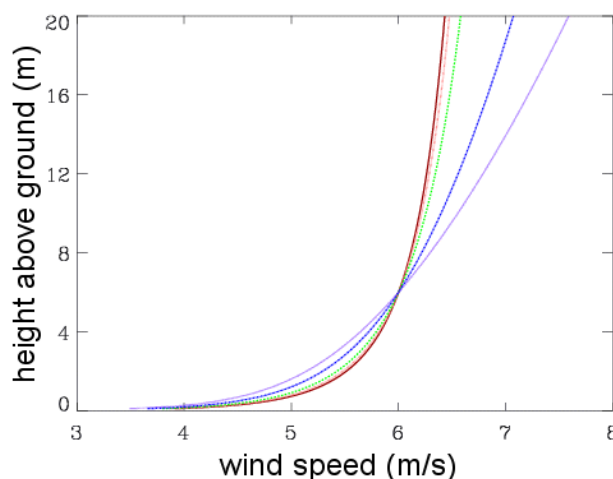


Figure 7: Typical log wind profiles for a variety of roughness lengths

The wind speed at the boundaries was calculated depending on several factors:

- i) The height above ground level
- ii) The roughness length scale, which is used to calculate the zero-plane displacement
- iii) The free-stream wind speed, which is the wind speed high above and relatively undisturbed by ground features

This was codified in the following expression for wind speed as a function of height above ground level:

<sup>8</sup> L. Mahrt et al. Determination of the surface drag coefficient. *Boundary Layer Meteorology* #99, 2001.

$$u_0(z) = \frac{u_f}{K} \left[ \ln \left( \frac{z-d}{z_0} \right) \right]$$

Where  $u_f$  is the friction velocity,  $K$  is von Karman's constant,  $d$  is the zero-plane displacement, and  $z_0$  is the roughness length. However, for stability reasons it was necessary to ramp this value from 0 m/s to  $u_0$  over a period  $t_{ramp}$ , using the following formula taken from previous work modelling tidal straits flow<sup>2</sup>:

$$u(z,t) = \left\{ \begin{array}{l} \left( \frac{t}{t_{ramp}} \right) u_0 : t < t_{ramp} \\ u_0 : t \geq t_{ramp} \end{array} \right\}$$

For the best balance of stability versus computational time,  $t_{ramp}$  was set to 60s.

## Note

These boundary conditions do not explicitly generate turbulence. It was planned that site LIDAR spot measurements on site could be analysed to calculate characteristic eddy lengths in the turbulence, to be used with Fluidity's implementation of the Synthetic Eddy Method (SEM)<sup>9</sup>. Time constraints meant that this was not possible; it is hoped that this can be returned to at a later date.

Even though the inflow boundary conditions did not include turbulence, the Fluidity simulations ran with turbulence modelling through LES and Smagorinsky. Thus, any turbulence generated by land features or within turbine model itself was handled correctly.

## 2.6 Turbine model configuration

As noted before, the wind turbine chosen for simulation at the Myres Hill facility is a NEG Micon NM54, with a rated power output at 950kW. This had to be parameterised into the Heriot Watt model prior to simulation.

### 2.6.1 Main specifications

These came from three sources:

- i) A NEG Micon technical report supplied by Sgurr<sup>10</sup>.
- ii) The Danish Wind Industry Association's (DWIA) online wind turbine power calculator<sup>11</sup>, which provides power curves and other data on many commercial wind turbines.
- iii) The OS coordinates of the turbine were supplied by Sgurr, so that it could be positioned within the simulation domain.

In Table 2 we can see a list of the main specifications of the NM54 turbine. These main parameters were fed into the central turbine configuration file, *turbines.dat*.

<sup>9</sup> Jarrin et al. A synthetic-eddy method for generating inflow conditions for large-eddy simulations. *Int. Journal of Heat and Fluid Flow* #27, 2006.

<sup>10</sup> NM54 Main Specification. *Technical report*. NEG Micon, 2004.

<sup>11</sup> Danish Wind Industry Association home page. Website. <http://www.windpower.org>

Property	value
Swept radius	27.25 m
Number of blades	3
Blade length	26.5 m
Blade twist	20°
Rotor shaft tilt	5°
Blade profiles	NACA 63.4xx, 63.2xx
Tip speed	63.9 m/s
Max. chord length	2.47 m
Hub height	55 m
Relative position (East, North)	( 3036 m, 3000 m )
Model hub altitude (rel. to origin)	219.96 m
Rated power	950 kW
Windspeed (max power)	~14 m/s

**Table 2: list of NEG Micon NM54 specifications**

### 2.6.2 Blade geometry

Turbine blade geometry within the turbine model is specified within a separate file named in *turbines.dat* as *nm54-geometry.dat*. It is specified as an ASCII file consisting as a list of tuples with three ordinates:  $r'$ ,  $\beta$  and  $c'$ . These are

- the normalised distance from the hub centre,  $r' = \frac{r}{R_T}$ .  $R_T$  is the swept turbine radius.
- $\beta = \beta(r')$ , the local blade chord twist in degrees
- $c' = \frac{c(r)}{R_T}$ , the normalised local chord length.

Drawing on the specifications in Table 2, and from inspection of the specification schematic in

Figure 8, reasonable estimates of  $r'$ ,  $\beta$  and  $c'$  were specified from  $r' = \frac{r_{hub}}{R_T}$  through to  $r' = 1$ . The estimates used are shown in Figure 9.

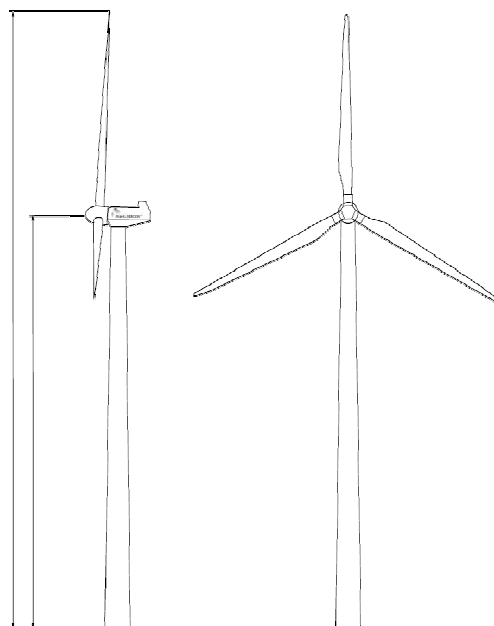


Figure 8: NM54 schematic

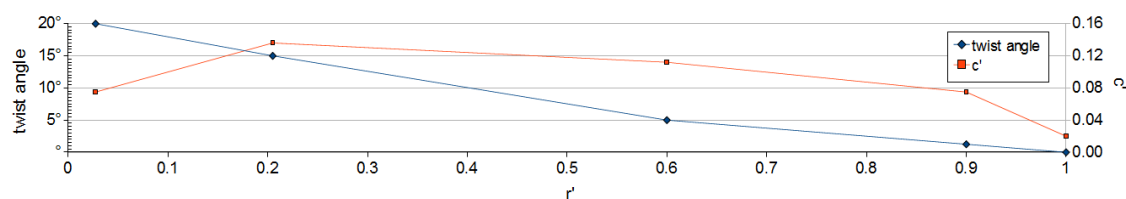
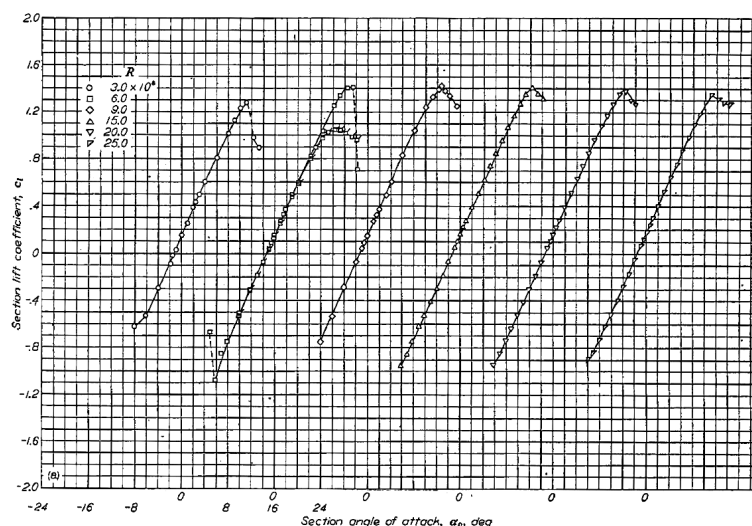


Figure 9: blade geometry - normalised radial length vs. twist angle and normalised chord length

### 2.6.3 Lift and drag characteristics

The NEG Micon specification lists the aerofoils used as NACA 63.4xx and 63.2xx. These are classifications from the National Advisory Committee for Aeronautics (the precursor to NASA), and as a U.S. government body its reports are in the public domain. The report that covers the lift and drag characteristics for the 6-series<sup>12</sup> (an example of lift coefficient graphs is given in Figure 10), and this was used to glean lift and drag characteristics of the turbine blades used in the NM54.

<sup>12</sup> The effects on variations in Reynolds number on the characteristics of a number of NACA 6-series airfoil sections. *NACA technical report #964* (1948).



**Figure 10: Lift coefficients of a NACA 63.xxx series aerofoil**

These were then parameterised as a table within a file named *nm54-liftdrag.dat*, which specifies lift and drag as a function of angle of attack (assuming Reynold's numbers  $\gg 10^4$ ). Since no precise specifications were available for the turbine aerofoils – there is no lift or drag data beyond an angle attack of  $20^\circ$  – a number of graphs had to be interpreted to produce the final lift and drag coefficients. Figure 11 shows the lift/drag coefficient graphs for the model turbine blades.

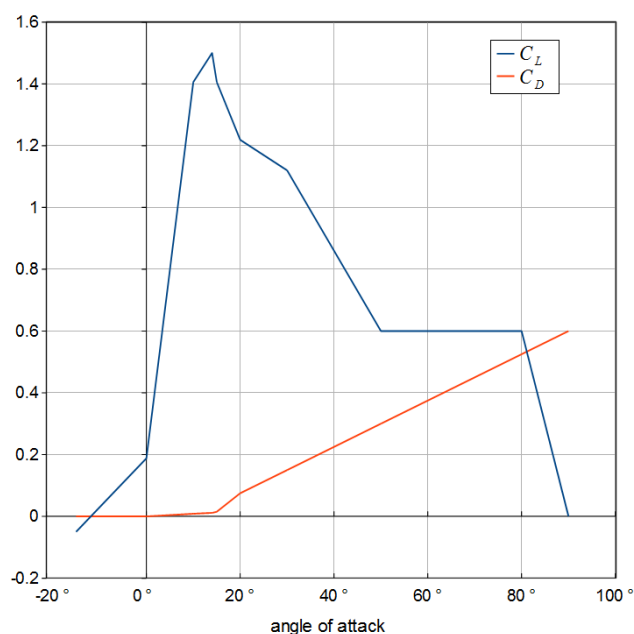


**Figure 11: angle of attack vs. lift and drag coefficients for the model aerofoil**

## 2.6.4 Turbine control mechanisms

### Dynamic blade pitch

The blade pitch  $\alpha$ , which is here measured relative to the rotor plane, is varied from an initial value  $\alpha_0$  of  $90^\circ$  (parallel, and heading into the wind), through to an

optimum target value  $\alpha_{opt}$ . This is done over a longer period  $t_\alpha$ . Thus at time  $t$  the blade pitch is specified as

$$\alpha(t) = \begin{cases} \alpha_0 - \left( \frac{\alpha_0 - \alpha_{opt}}{t_\alpha} \right) t & : 0 < t < t_\alpha \\ \alpha_{opt} & : t \geq t_\alpha \end{cases}$$

After some experimentation, the optimum blade pitch was found to be  $\alpha_{opt} = -6^\circ$ . The blade pitching time was set to  $t_\alpha = 120$  s.

## Wind turbine orientation

The turbine model automatically orients itself toward the wind. Typically, it will start facing towards the wind at the boundaries, that is to say

$$\theta_T(t=0) = \theta_{wind}(t=0)$$

However, due to turbulence, topographic and ground effects, beyond the boundaries and deep within the mode,  $\theta_{wind}$  will deviate from its initial value. Thus  $\theta_T$  has to be controlled to ensure optimum performance of the model turbine, ie. to satisfy the condition.

$$\theta_T(t) \approx \theta_{wind}(t)$$

A slow turning pace was necessary to so that the model's orientation would not suddenly 'flip' in the face of turbulent flow, thereby inducing artificial oscillation and resonance within the fluid. Thus the maximum rate of turning was set to

$$\left( \frac{d\theta_T}{dt} \right)_{\max} = 1 \text{ deg/sec}$$

So in one time-step the maximum change in angle would be  $\Delta\theta_{T, \max} = \left( \frac{d\theta_T}{dt} \right)_{\max} \cdot \Delta t$

This gives one full rotation in 6 minutes, which is much faster and more responsive than the control mechanism on a real turbine. In terms of simulation run-time, it was not practical to use slower turning rates.

### 3 Results from simulation and experiment

This initial set of data was taken by Sgurr's Galion LIDAR device as the surface of a semi-cone with elevation of  $25^\circ$  as show in Figure 12. This semi-cone swept anti-clockwise from  $0^\circ$  (bearing north) to  $180^\circ$  (bearing south), and was averaged over 60 minutes.

Sgurr also provided a data file with (x,y,z) coordinates relative to Galion, and the wind-speed at each coordinate. With the Galion co-ordinates given as

$$(3106, 3000, 160)$$

(metres east, north and height from model origin), the data set could then be compared with data at similar coordinates within the model.

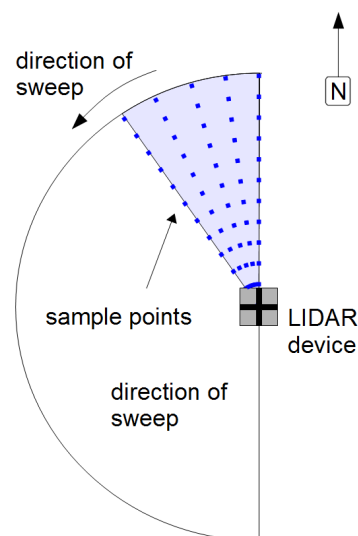


Figure 12: plan view of LIDAR sweep

#### 3.1 Notes on modelling

##### 3.1.1 Simulation run times

An hour of simulation time would take too long, so it was decided that the simulation would run for 10 minutes, which should give adequate time for the air flow to settle down into a dynamically stable state, such that averaged values could be taken. To aid this, the wind profile boundary conditions were not imposed immediately, but had a 'ramp time' of 2 minutes – starting at 0 m/s and gradually rising to their maximum value.

##### 3.1.2 Extrapolation of boundary conditions

To ensure that wind conditions are approximately the same at the wind turbine, the boundary conditions at the edge of the model had to be extrapolated from the LIDAR measurements. Appropriate conditions were set for the model were set:

- wind speed at hub height of approx. 6 m/s
- wind direction  $225^\circ$

From initial simulations, it was deduced that due to the effect of the logarithmic wind profile, the maximum free-stream wind speed should be set at approximately 8.0 m/s. It was assumed that the bathymetry would not significantly alter the general wind direction from the southern boundary to the wind turbine.

#### 3.2 Flow within the model turbine

This section describes the control processes within the turbine. The turbine model is designed to face towards the wind with a maximum rotation rate of 0.1 RPM, for slow but steady adjustment. Figure 13 justifies the choice of this maximum rotation rate – the turbine aligns itself into the mean wind within a time scale of around a minute, and then maintains that orientation despite minor fluctuations of the wind direction at a time scale of 10 s.

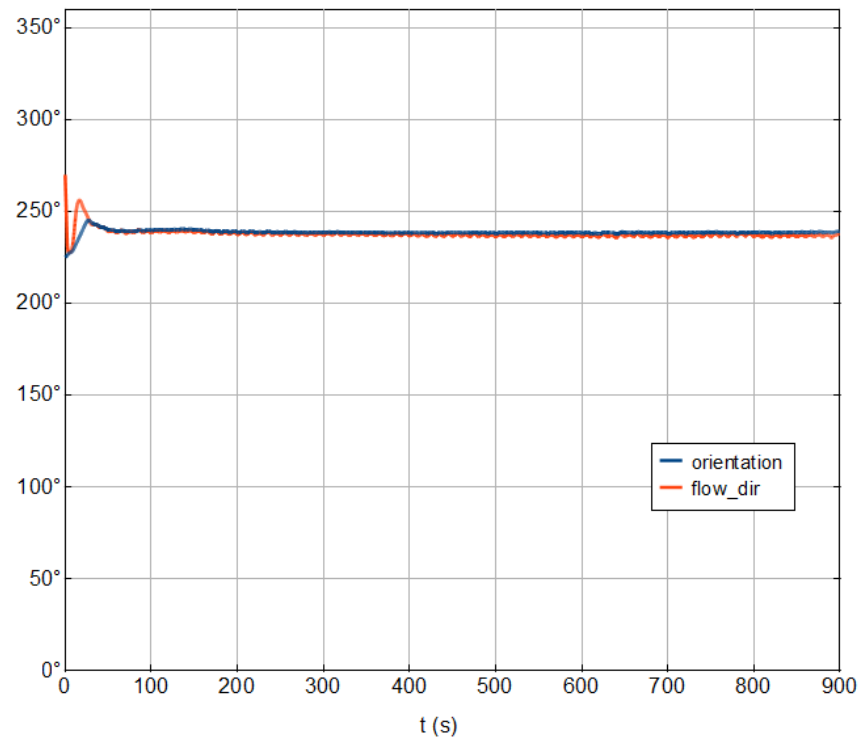


**Figure 13: time vs. flow direction (within turbine) and turbine orientation**

In Figure 14, we can see the blade pitch slowly decrease from 90° (parallel to the flow) to -6° (the optimum pitch). As the mean attack angle decreases, we can see a sharp acceleration in the blade angular velocity, until at 250 s it peaks.

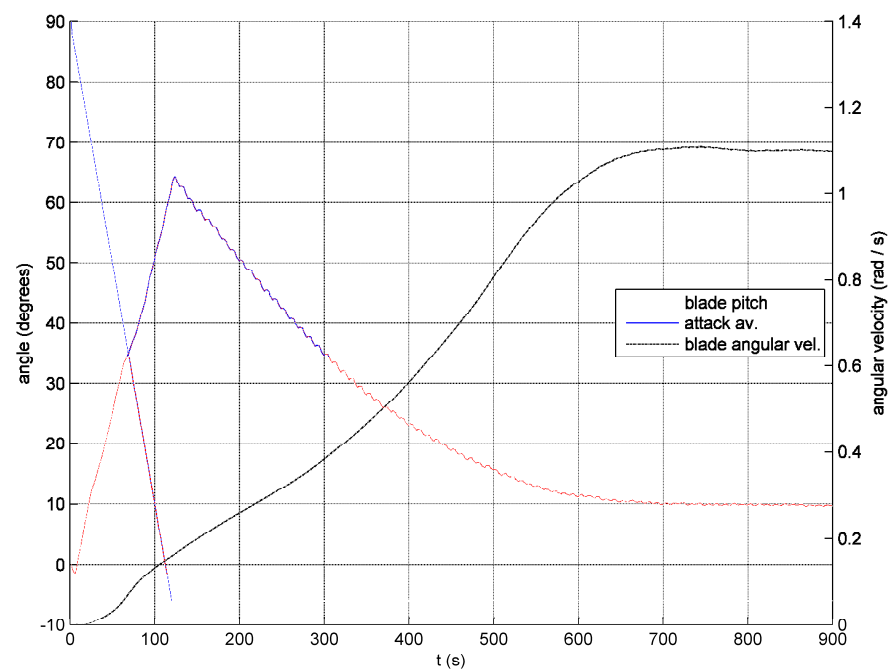


**Figure 14: time vs. blade pitch, angle of attack and blade angular velocity**

This can be explained by three conditions:

1. The lift varies as the square of the flow speed relative to the blade, thus there is a  $r\omega_r^2$  dependence.
2. As the mean angle of attack approaches the range for maximum lift (approx.  $10^\circ - 15^\circ$ ), the torque acting on the fluid increases: this has an interdependence with condition 1 above.
3. At  $t = 250$ s the generator torque balances the fluid torque, and the turbine blades cease to accelerate.

### 3.3 Power output and torque

Unfortunately, access to real-time performance data produced by the Micon turbine was not possible. However, we can use official statistics to ascertain what the power output should be. According to NEG Micon's specification report<sup>10</sup>, the power output at 6 m/s is 105kW. The model produces second-by-second power output, which due to time-dependent flow conditions will vary as the simulation progresses. We can see from Figure 15 it levels out to round 43kW; this discrepancy will be discussion in section 4.1.1.

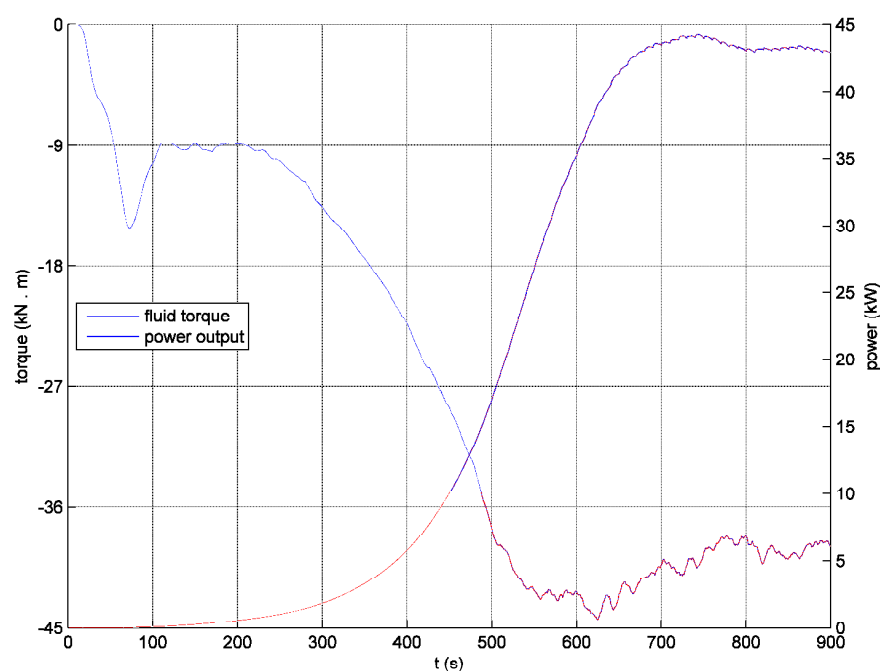


Figure 15: power output and fluid torque over time from modelled Micon turbine

We can also note that the sharp increase in power matches closely with the fluid torque peak amplitude, which from Figure 14 matches the period the mean attack angle approaches its optimum value.

### 3.4 Wake results

Due to the nature of the data – a curved slice – straightforward wake deficit plots were not possible. However, it was possible to take 2D projections of the experimental and LIDAR data (by zeroing the vertical co-ordinate), and plotting wind speed contours.

#### 3.4.1 The LIDAR wake data

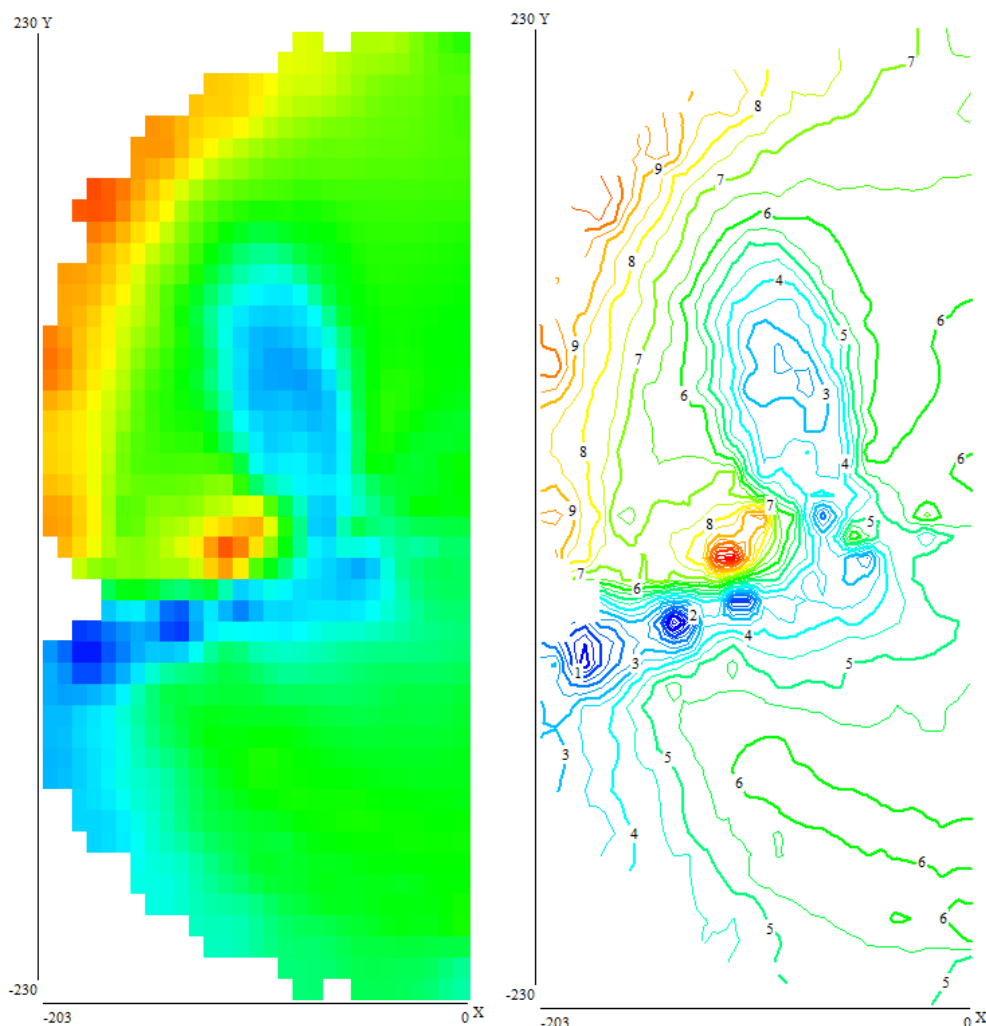


**Figure 16: the colourmap and contour plots of wind speed from LIDAR data, with the axis values in metres. Air flow coloured dark blue is slower than red. The contour values are windspeed in m/s.**

From Figure 16, we can see the wake behind the Micon stretch northwards, immediately up and right of the red spot. The air flow around the turbine can be roughly characterised as below:

- The overall speed of the flow is around 5-7 m/s, although this increases to upwards of 8 m/s further north. This almost consistently lies on the periphery of the LIDAR sweep: if we return to Figure 6, we can see this equates to the ground covered by trees. This may be down to the local flow acceleration over these trees due to the blockage effect.

- The three dark blue points are suspected of being the result of interference from surrounding masts and other building structures at the Myres Hill test facility (hopefully Sgurr will confirm this). Figure 17 seems to suggest some out-lying buildings, and possibly masts: further discussion will be needed with Sgurr to clarify.
- The wake deficit reaches to around 2.5 m/s at a horizontal distance of 1-2 diameters downwind. Note, that because the measurement height coordinates increase with distance from the LIDAR device, they will rise above the extent of the turbine wake. This means it appears shorter than it actually is, since wind speeds will be greater outwith the turbine wake.



**Figure 17: Google(tm) satellite view of Myres Hill. The Micon turbine is highlighted.**

We can also calculate some rough metrics over our pseudo-wake. If we draw a line from the Micon down through the middle of the wake (see Figure 18), we can find the approximate wake direction.

If the turbine is taken at horizontal co-ordinates (-70m, 0), and the edge where wake recovers to the hub-height freestream velocity, 6 m/s, at (-103m, 143m), then we can write the anti-clockwise angle from due north as

$$\begin{aligned}\theta_{wake} &= \tan^{-1}\left[\frac{b}{a}\right] \\ &= \tan^{-1}\left[\frac{103-70}{143}\right] \\ &\approx 13^\circ\end{aligned}$$

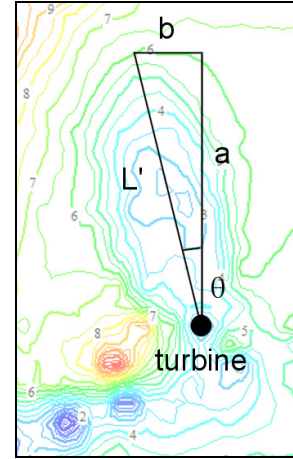


**Figure 18: calculating LIDAR wake metrics**

This means that the wind heading can be estimated as

$$\theta_{wind} = 167^\circ$$

We can then calculate the pseudo length of our wake – *pseudo*, as it does not reflect the actual length of the wake, since the wind speed measurements are not from a constant height, ie. hub height. We write this pseudo length as

$$\begin{aligned}L' &= \sqrt{(a^2 + b^2)} \\ &= \sqrt{(143^2 + 33^2)} \\ &\approx 147\text{ m} \\ &\approx 2.7\text{ diameters}\end{aligned}$$

We can use this information to produce a profile to directly compare the wake structure behind the real turbine with the model – more on this in subsection 3.4.3.

### 3.4.2 The turbine model wake data

The model wake data was averaged over the last 2 minutes of simulation, when the power output and wake had stabilised. To ensure that similar parts of the wake were being inspected, the scan coordinates were rotated  $70^\circ$  anti-clockwise about the turbine, to ensure that similar parts of the wake were being compared. You can think of this as moving LIDAR equipment north and west, whilst keeping it pointed towards the turbine and at the same distance.

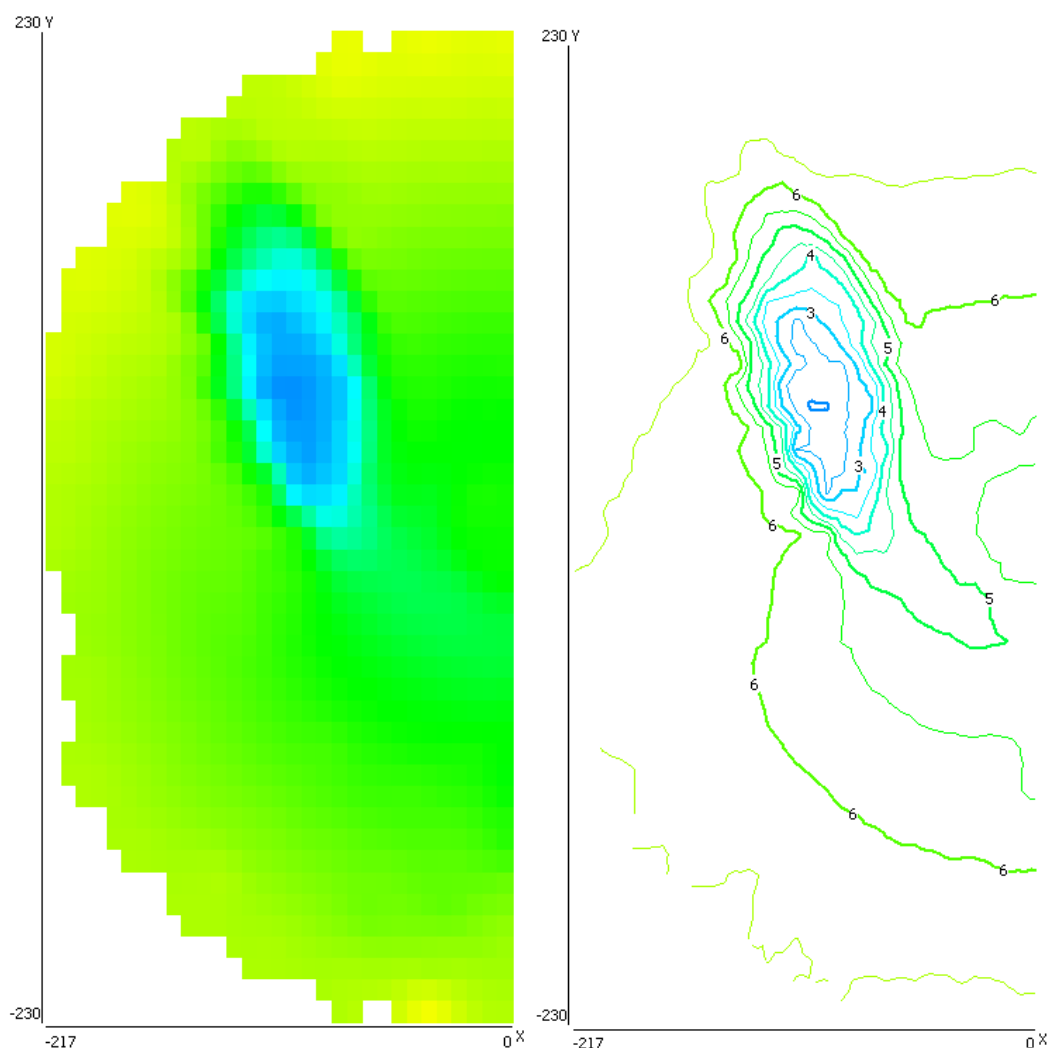


**Figure 19: the colourmap and contour plots of wind speed from the model.**  
**Dark blue represents lower wind speeds. The contour values are windspeed in m/s.**

In Figure 19 we can see the colour map grid of wind speed, and the corresponding contour map. First thing to note is that the wakes, whilst not in precisely the same orientation, have broadly the same characteristics as the LIDAR measurements. Immediately, we can notice some discrepancies:

- The wake wind speed deficit is similar to that of the measured wake, dropping to approximately 2.5 m/s.
- The three dark blue spots in the LIDAR data in Figure 16 are not present in the model colour grid, which is much smoother. This is not surprising, as smaller ground features are not discretely modelled. Doing so is possible, but would require an increase in model resolution. Currently the minimum element length is 7.5 m; reducing this to 2m, say, would require reducing the time step size and increasing the number of elements in the simulation.

There are also some broad similarities to highlight:

- The mean hub-height freestream wind speed sits at around 6-7 m/s.

- On the upper left periphery, the wind speed increases to well over 8 m/s – this is partially down to increase in scanning height, but as the increase is more pronounced here than in the southern section, we can assume that the increased drag due to trees north of the turbine is having an effect (clearly shown in Figure 17).

To calculate some metrics of the wake, we draw a line along the approximate centre of the wake from the turbine, to where the wind speed recovers to 6 m/s. Relative to the LIDAR device, this occurs at (-54m, 163m). From this we have

$$\begin{aligned}\theta_{wake} &= \tan^{-1}\left[\frac{-b}{a}\right] \\ &= \tan^{-1}\left[\frac{60}{170}\right] \\ &\approx 19^\circ\end{aligned}$$

This means that the wind heading can be estimated as

$$\theta_{wind} = 234^\circ$$

(We can see this is clearly ‘off’ the  $\theta_{wind} = 225^\circ$  specified at the boundaries – most likely due to topographical and ground feature effects.)

Calculating our pseudo wake length gives us:

$$\begin{aligned}L' &= \sqrt{(a^2 + b^2)} \\ &= \sqrt{(170^2 + 60^2)} \\ &\approx 180m \\ &\approx 3 \text{ diameters}\end{aligned}$$

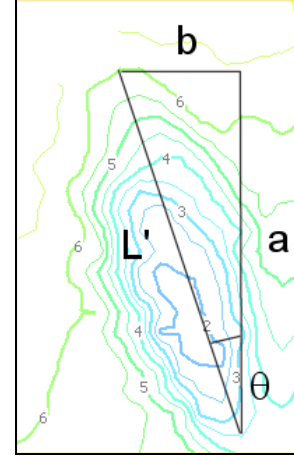


**Figure 20: calculating model wake metrics**

### 3.4.3 Comparison of wake profiles

In Figure 21, we can see the structure of the wakes along the line denoted  $L'$  for the LIDAR measurements and the model results. This marks the changes in wind speed along that line; it should be noted that in reality this line is not straight – it is a curve on the surface of the semi-cone that represents the Galion LIDAR scan. As such, it will be difficult to intuit the overall structure of the wake and the wake recovery length. Nonetheless, it gives a method to directly compare measurement with simulation.

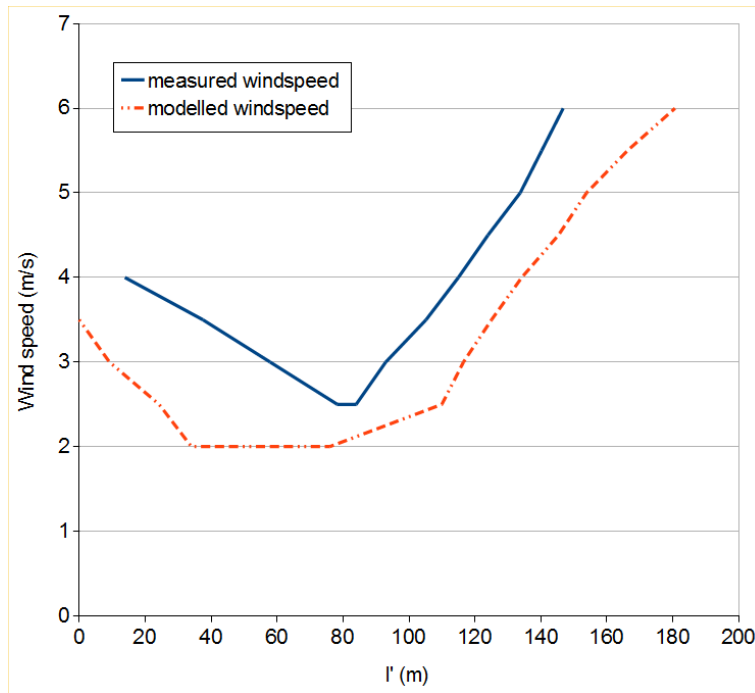


**Figure 21: comparison of wake structures between model and measurement. The dashed line represents the model. The distance along the line  $L'$  is denoted  $l'$ .**

Despite a difference of almost  $67^\circ$  in wind direction at the turbine, it can be seen that the model follows the profile of the measured data, albeit approximately with a slightly deeper, broader velocity deficit.

1. An error in the LIDAR instrument co-ordinates. These will be re-checked with Sgurr at the final meeting due 10<sup>th</sup> August 2009.
2. Even with the rotation and translation of the LIDAR measurement points in the simulation, the difference in wake directions means that the height of each of the comparative points along  $L'$  will be slightly different – lower points are associated with lower wind speeds.
3. Different wake structures. As has been mentioned turbulence is modelled within the simulation domain (eg. blade and ground-generated turbulence), but not at the boundaries per se. This ambient turbulence this is known to have an influence on wake structure<sup>1</sup>; more will be said on this in section 4.

### **3.5 Model flow visualisation**

This subsection will deal with additional data from the model that could not be compared with the LIDAR data, but demonstrates a) the capabilities of the model, and b) what can be compared with more detailed sets of LIDAR data in the future.

#### **3.5.1 Horizontal slice**

In this section, we take a two-dimensional, horizontal slice through 3D data set, centred upon the hub of the wind turbine, at specific time intervals of  $t=\{0s, 60s, 120s, 300s, 900s\}$ .

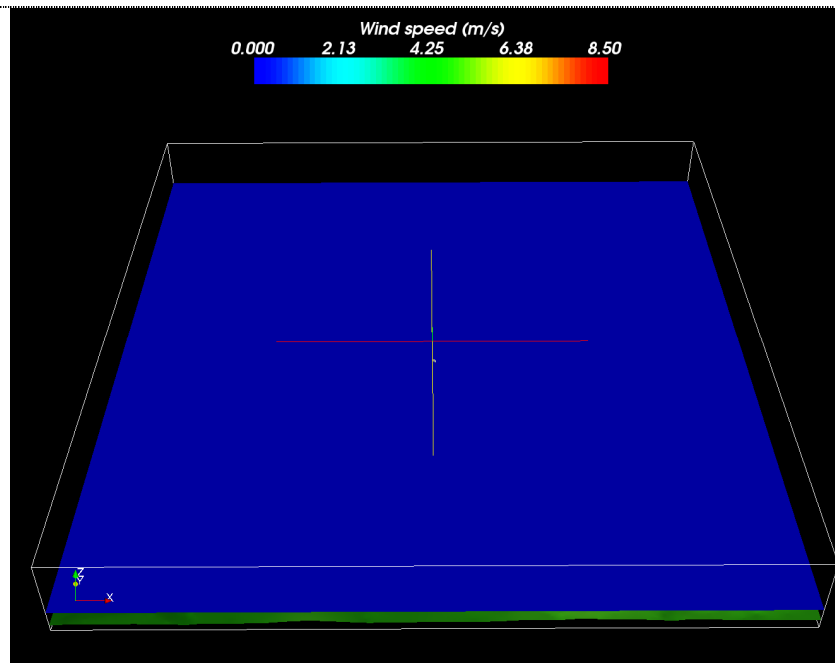
## Large scale

The views are above and slightly to the south of the model domain. They show the whole simulation domain, measuring 6km x 6km x 750m.

**t=0s**

Boundary and internal flow conditions set to  $u=0$  m/s.

The turbine can just be seen below the central cross-hair.



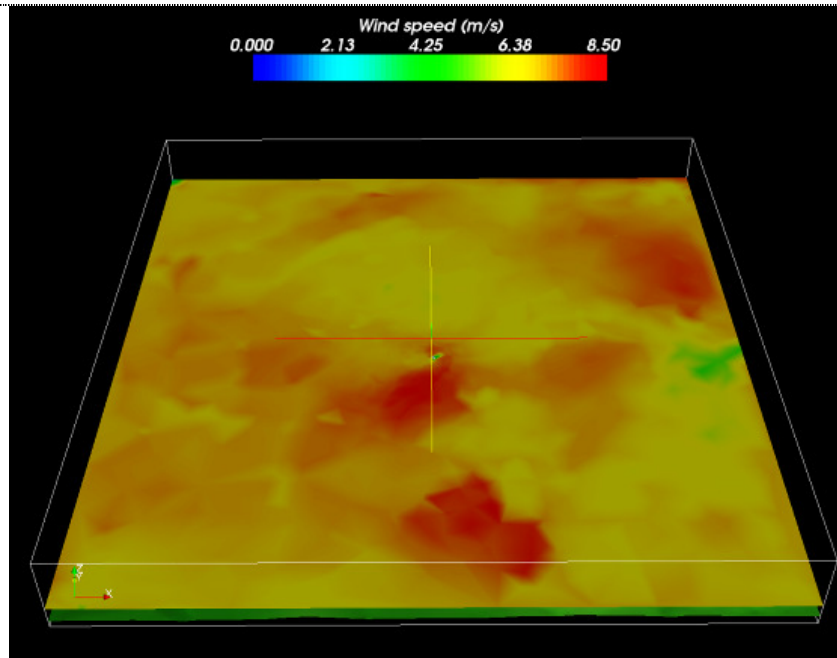
**t=60s**

Boundary conditions are now

$$u(z,t) = u_0(z).$$

Areas of fast-moving flow due to gradient speed-up can be seen.

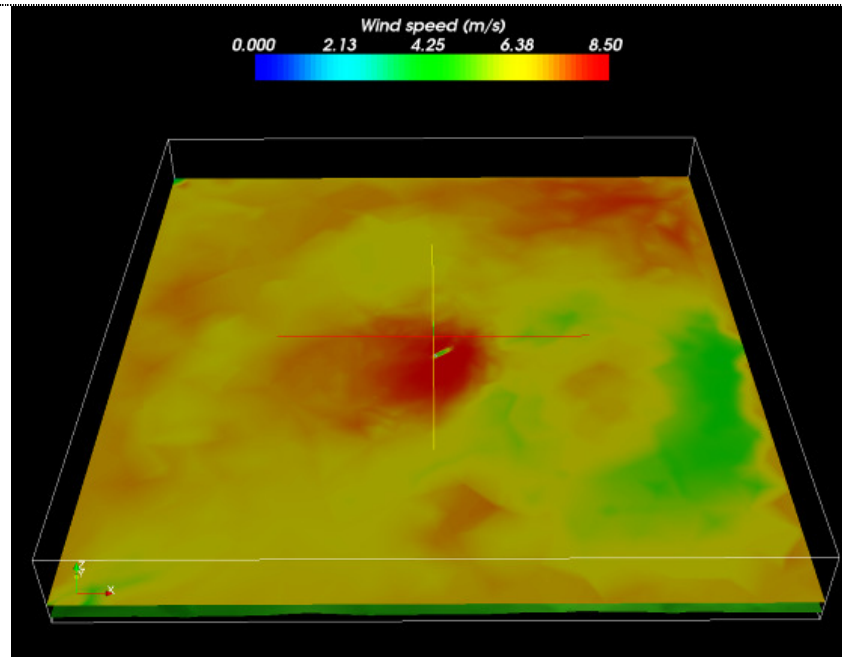
The turbine itself is placed at the end of a ridge; the wake can be seen behind it, slowly starting to develop.



**t=120s**

The flow has begun to settle down; the speed-up around the turbine and surround ridge is still noticeable.

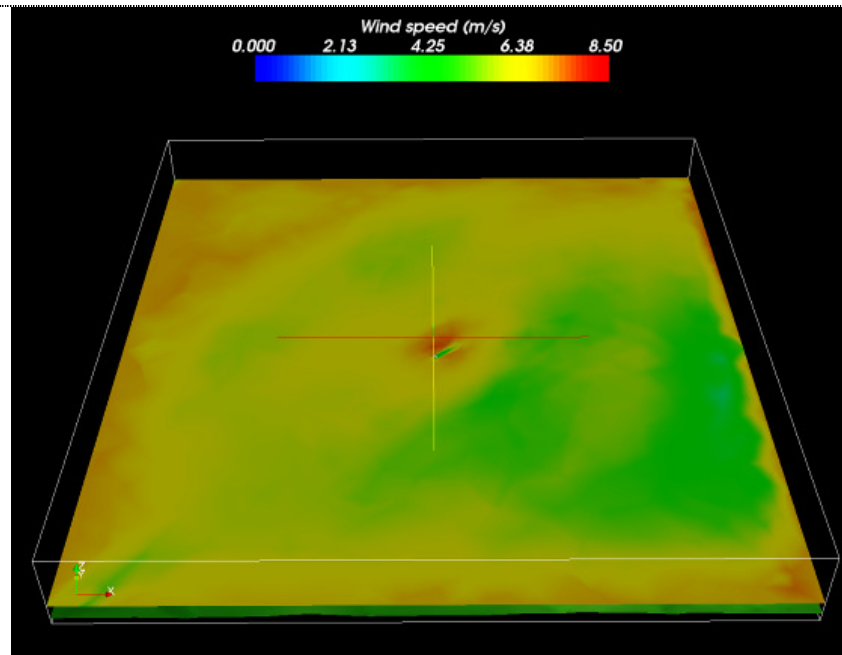
The wake behind the turbine has almost doubled in length.

**t=300s**

Air flow approaching dynamically steady conditions.

Turbine wake has nearly doubled in length again.

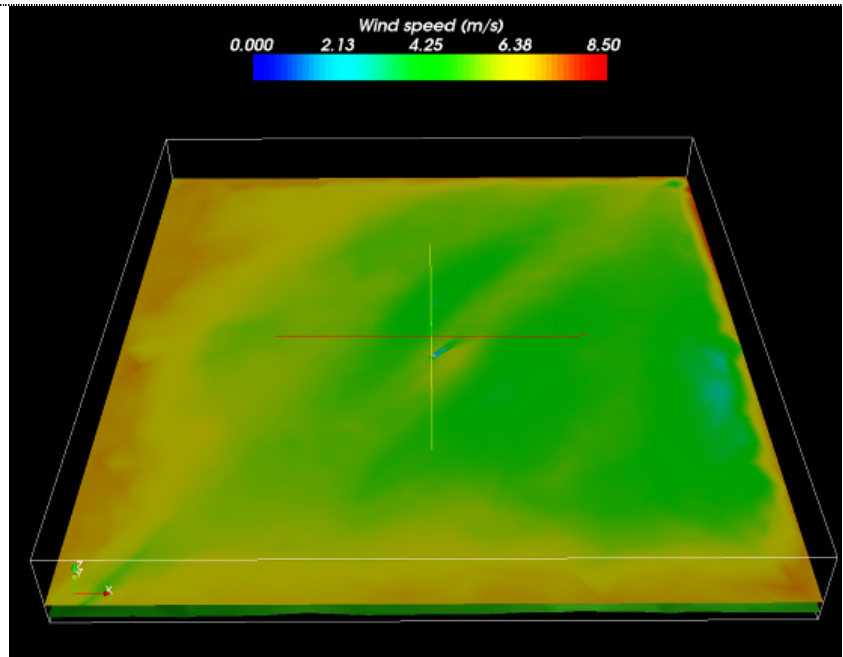
Slightly discrepancy between boundaries and model conditions noticeable.



**t=900s**

Flow has now reached very steady state; friction effects due to ground features coming into play, slowing air-flow near ground.

Turbine is surrounded by forestry on exposed ridge; speed up is still visible at turbine location.

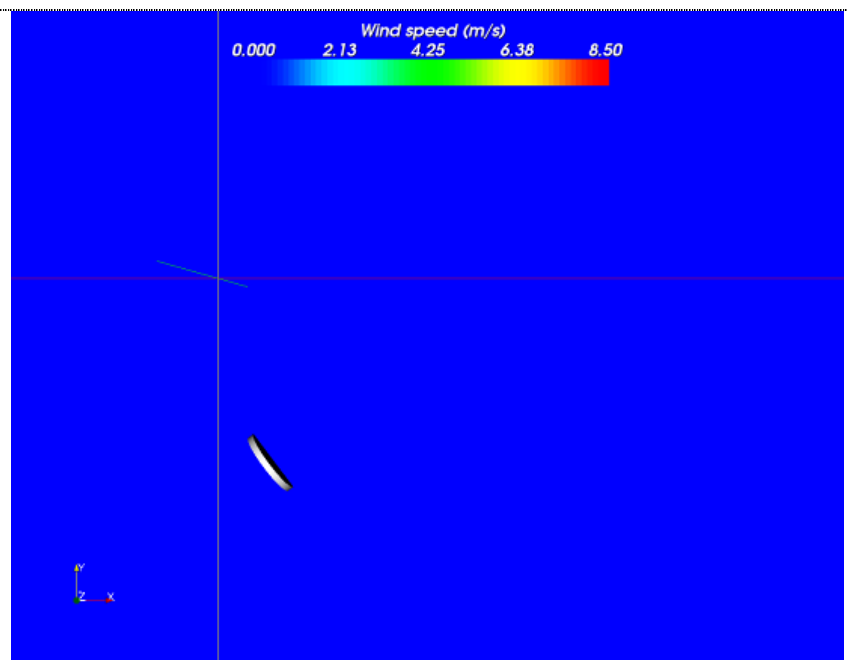


## Local view

To show a little more detail in the flow, these are viewed from directly overhead and zoomed in – the slides measure approximately 1100m x 520m.

**t=0s**

No air moves across the ridge or through the turbine – the boundary conditions are set at  $u=0\text{m/s}$ .

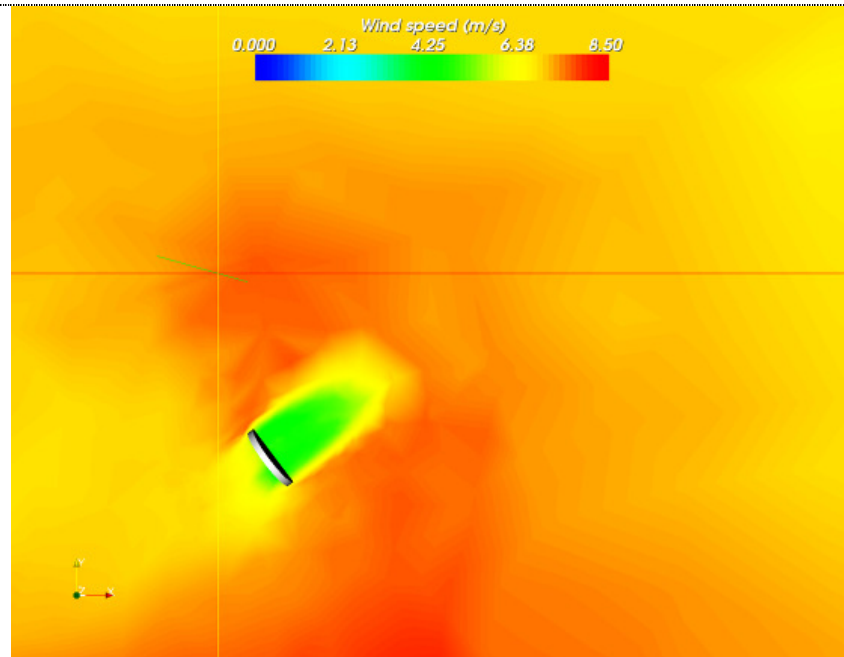


**t=60s**

Boundary conditions are now at their maximum values.

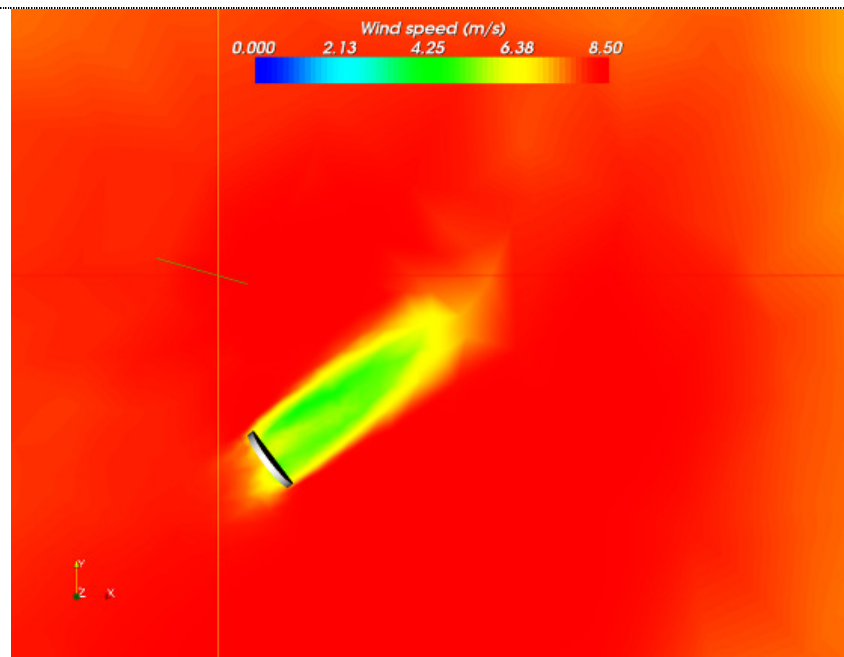
The flow accelerates around the turbine due to the blockage effect.

The turbine is not facing 225°; topography has affected the wind direction.

**t=120s**

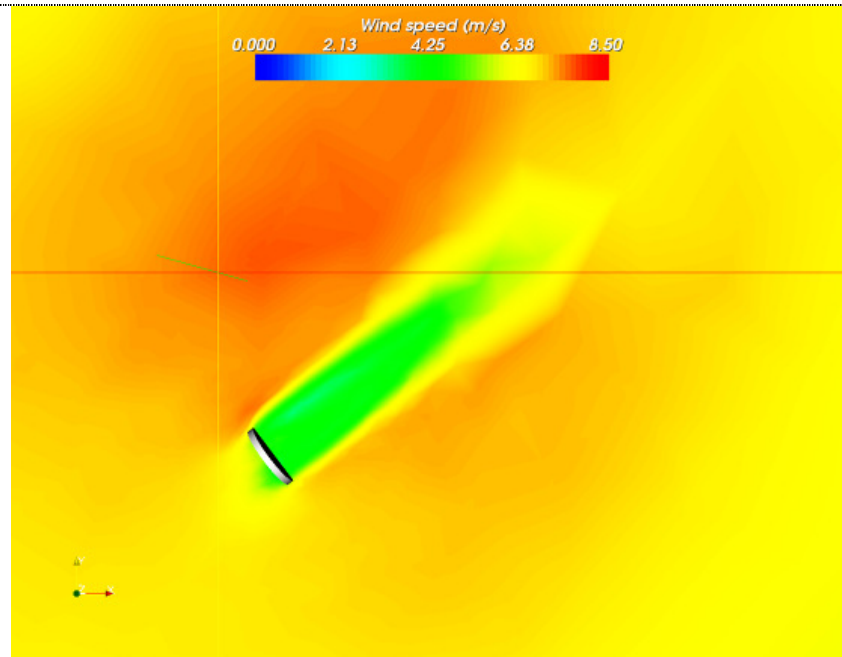
Wind speed surrounding turbine much higher (possibly higher than 8.5 m/s – colour scale was kept constant through visualisation).

Air flow can be seen slipping through hub region, main deficits are approximately  $r=(3/4) R_T$ .



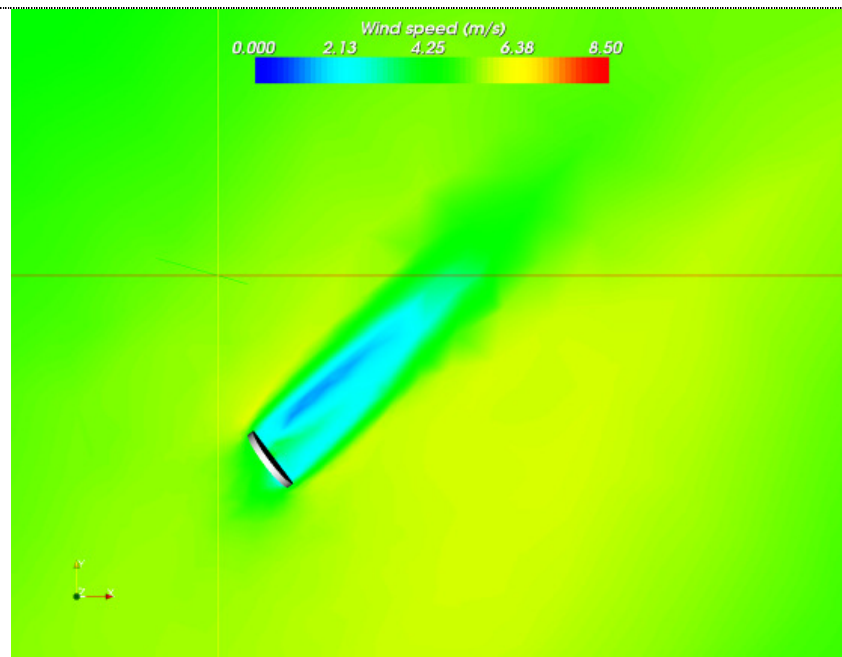
**t=300s**

Air flow has actually slowed over ridge slightly – ground feature friction competes against gradient speed-up (this will become clearer in the vertical slices shown later).

**t=900s**

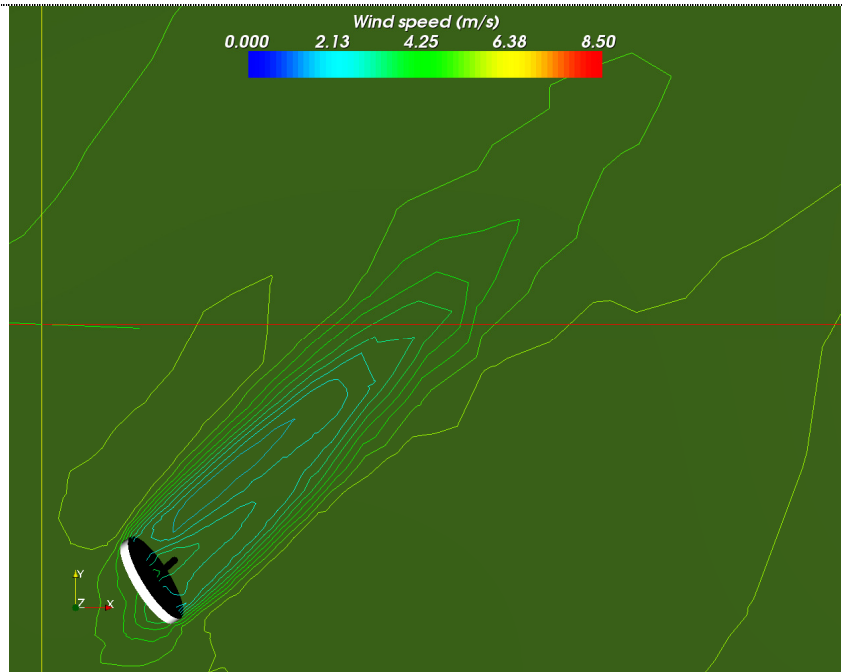
Air flow has slowed yet again. Blockage speed-up around turbine still visible.

Also note that the greater velocity deficit (1-2 m/s) on the right side of the turbine wake: this is due to a slight misalignment of the turbine into the wind.



**Contour plot at  $t=900s$** 

This shows the wake structure behind the turbine more clearly.

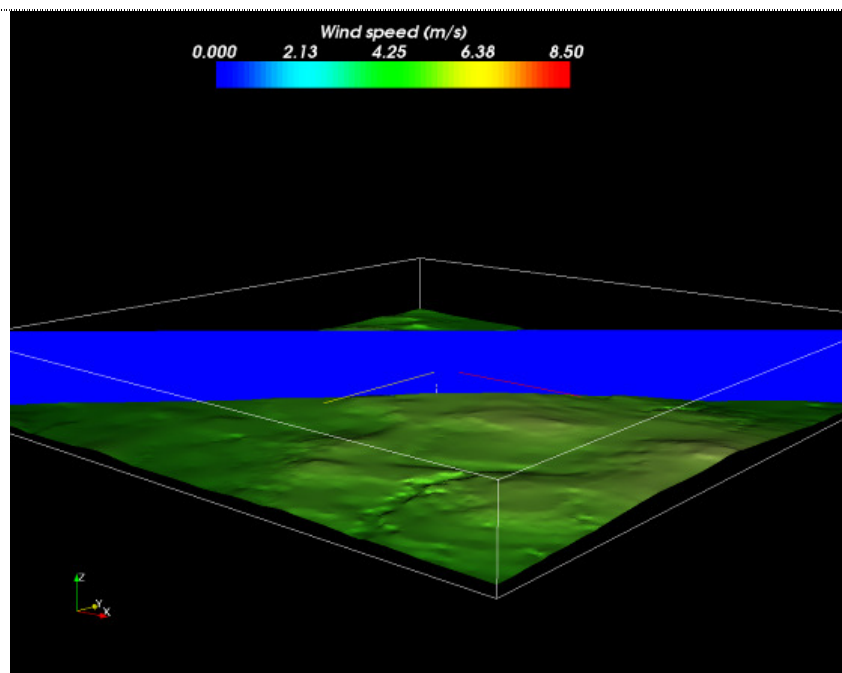
**3.5.2 Vertical slice**

Here we have a two-dimensional vertical slices through the 3D data, again centred upon the hub of the wind turbine. The views are ‘snapshots’ at  $t=\{0s, 60s, 120s, 300s, 900s\}$ .

**Large scale** **$t=0s$** 

View of the vertical slice from the southeast, looking northwest towards the wind turbine.

The turbine is almost dead centre, where the cross-hairs meet.

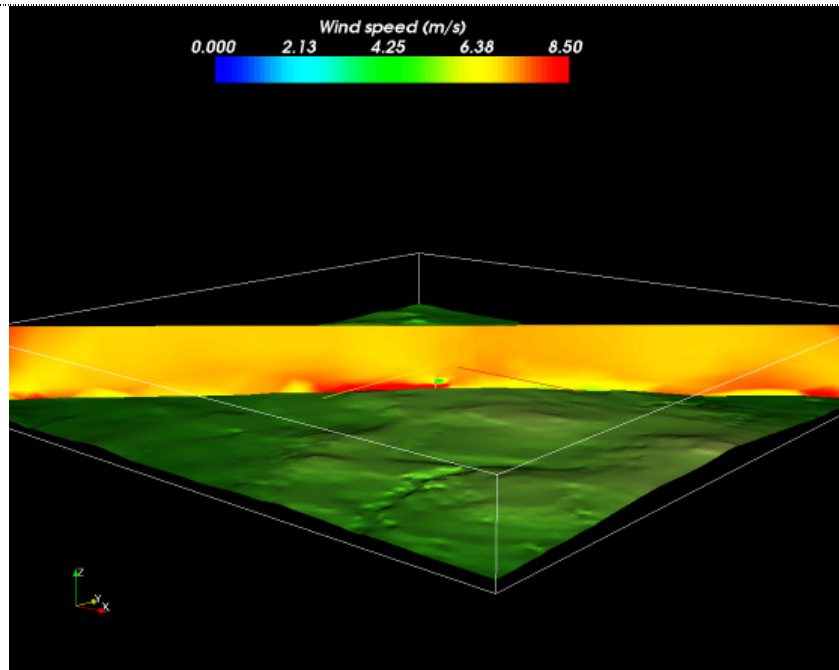


**t=60s**

In the centre we can see the wake start to form behind the turbine.

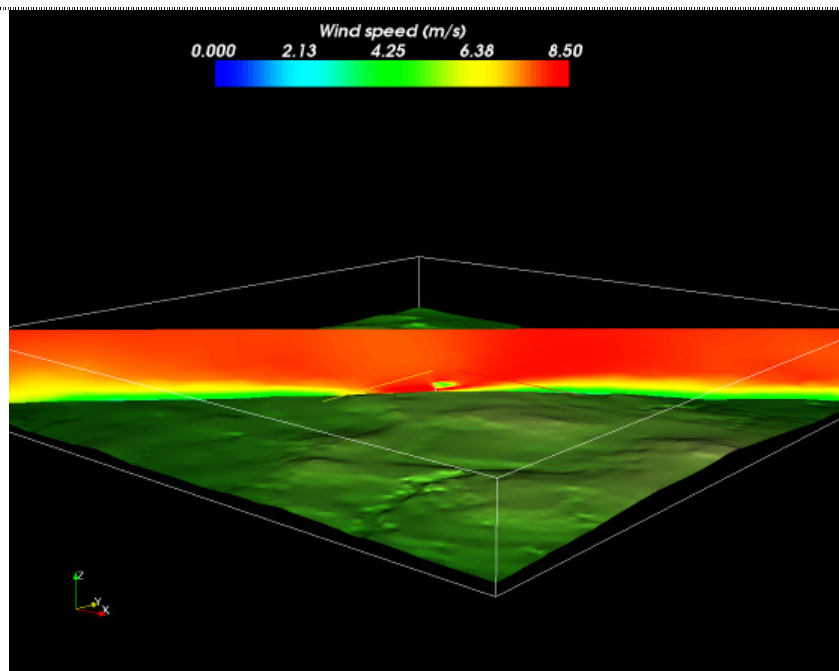
Before the turbine (southwest, left), we can see the speed-up due to an upward land gradient.

On the right (NE), we can see a slow down partially due to the downward gradient.

**t=120s**

The turbine wake has doubled in length, and the effects of friction due to ground features come to the fore.

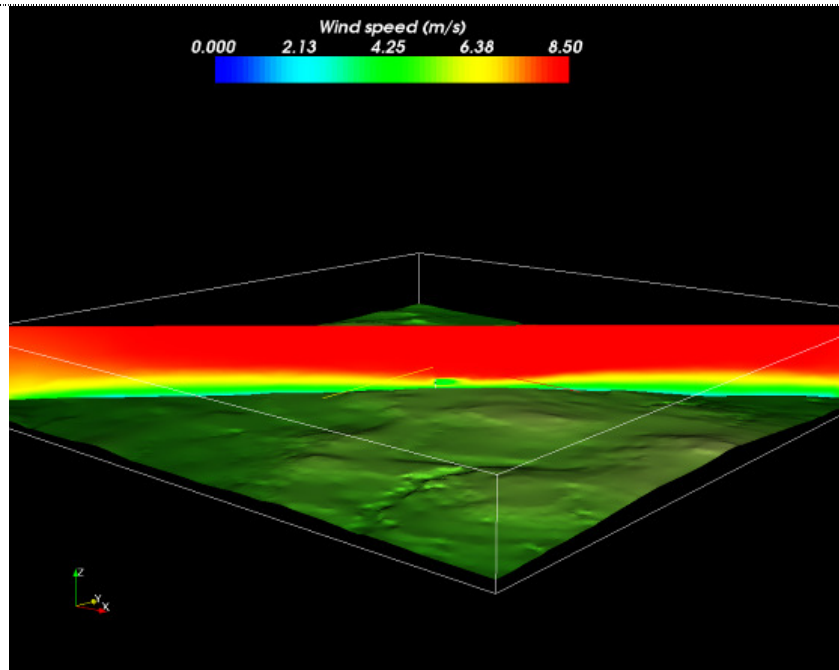
To the SW and NE of the turbine is forestry, and we can see its effect on the vertical wind speed gradient.



**t=300s**

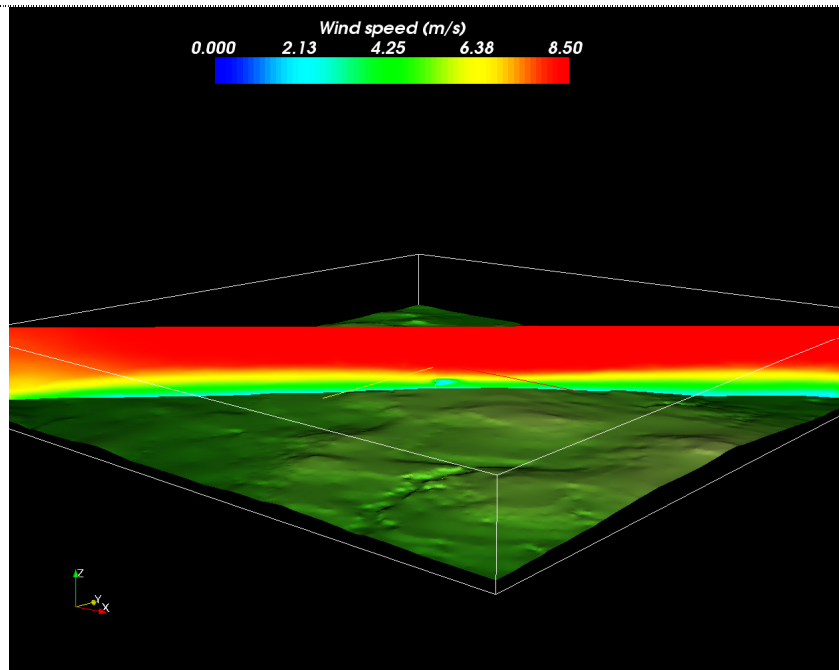
Even though the immediate area surrounding the turbine only consists of rough grass with a much lower drag co-efficient, the forestry clearly restricts the air-flow down-wind.

The land gradient speed-up has now all but disappeared.

**t=900s**

The air flow has now settled into dynamic stability.

Wind speed over the turbine ridge remains higher than the surrounding environs due to its exposed outlook.



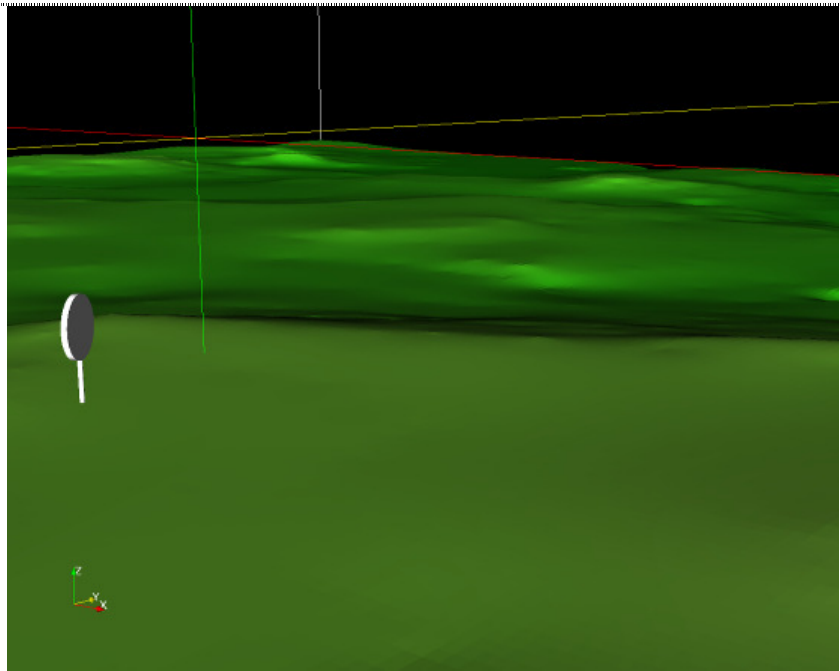
## Local scale

### Reference view

To give an idea of the context, this is a zoomed-in view, looking northwest towards the turbine.

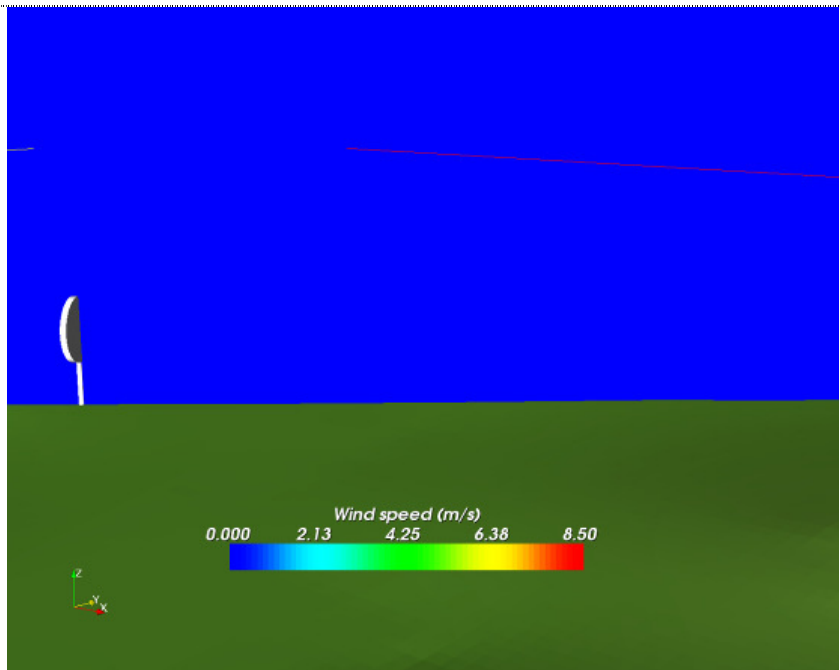
Right of the turbine is an extent of 1 km.

Beyond the turbine, we can see the sharp descent of the far side of the ridge.



### t=0s

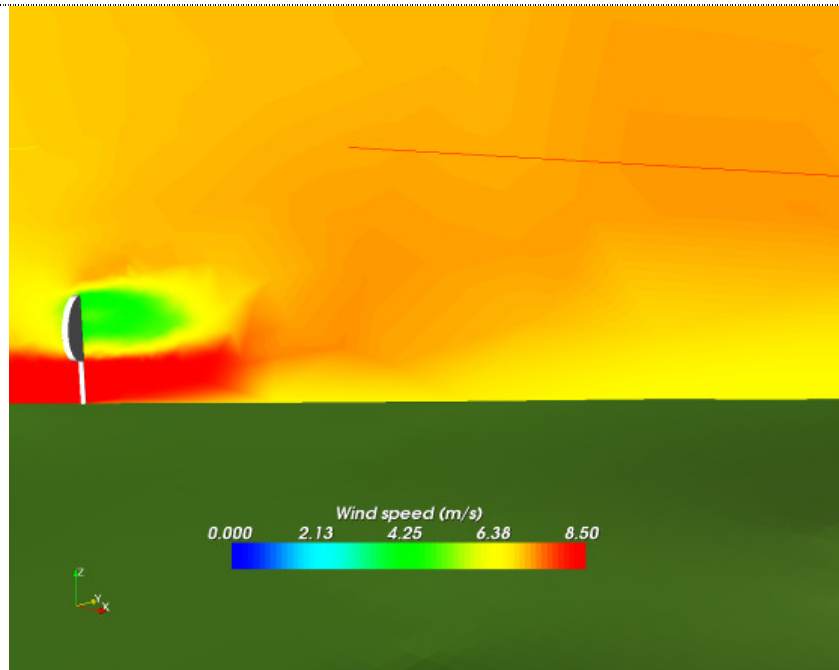
Imposition of 2D vertical slice on previous view.  
No air flow.



**t=60s**

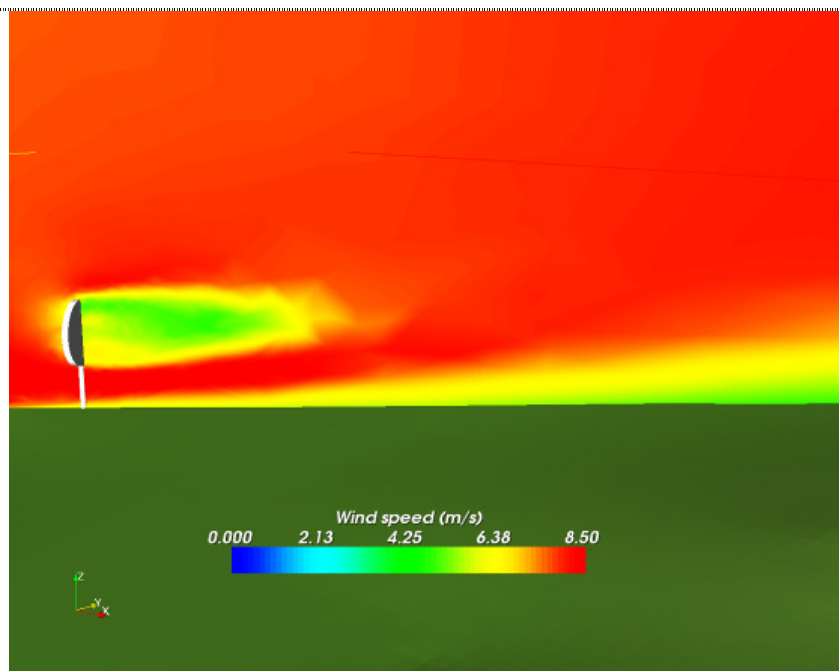
This view shows the wake starting to evolve, and the gradient based speed-up of  $>8.5\text{m/s}$ . To the left, the ridge falls away.

This speed-up would lead to the turbine blades rotating too quickly; hence the blade pitch control was necessary for stability.

**t=120s**

The turbine wake has doubled to around 4 turbine diameters.

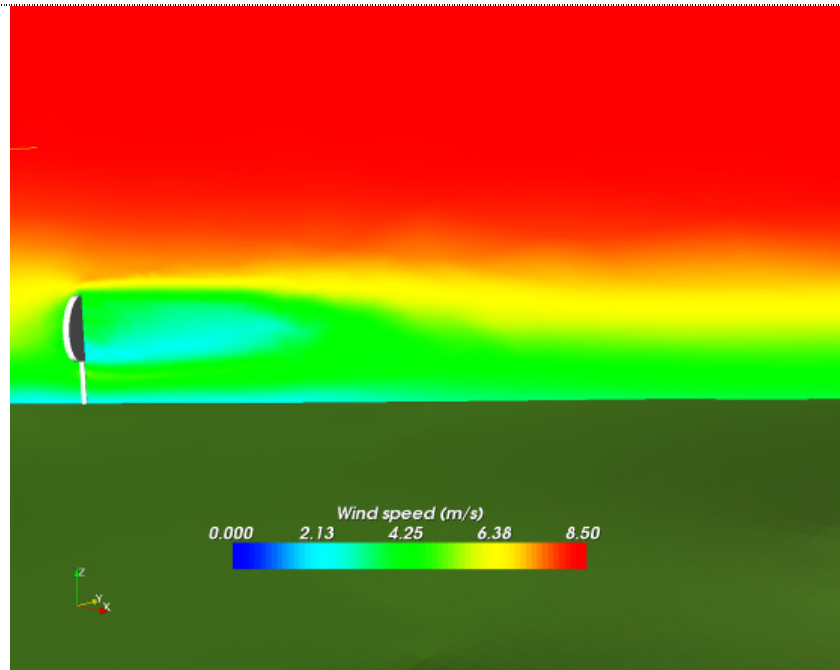
The land gradient speed-up is sweeping over the ridge. At this stage though, the increased drag due to trees to the northwest starts to impose a vertical velocity gradient upwind.



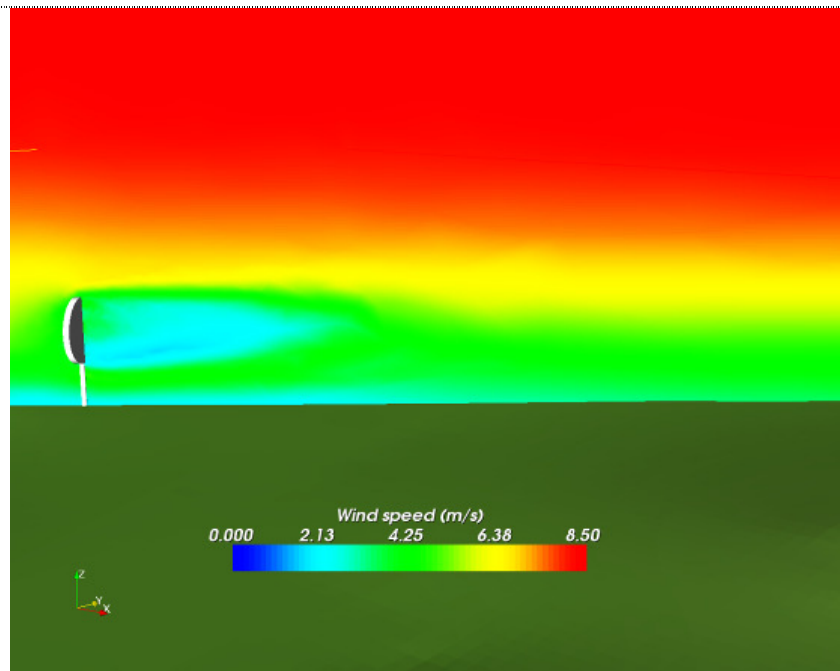
**t=300s**

The ground effect (drag) of trees both down-wind (southwest, left) and up-wind (northeast, right) has imposed a vertical wind speed gradient, reducing flow at hub height to around 5-6 m/s.

Secondly, the rough grass has created drag beneath the turbine, reducing flow near the ground to approximately 2 m/s.

**t=900s**

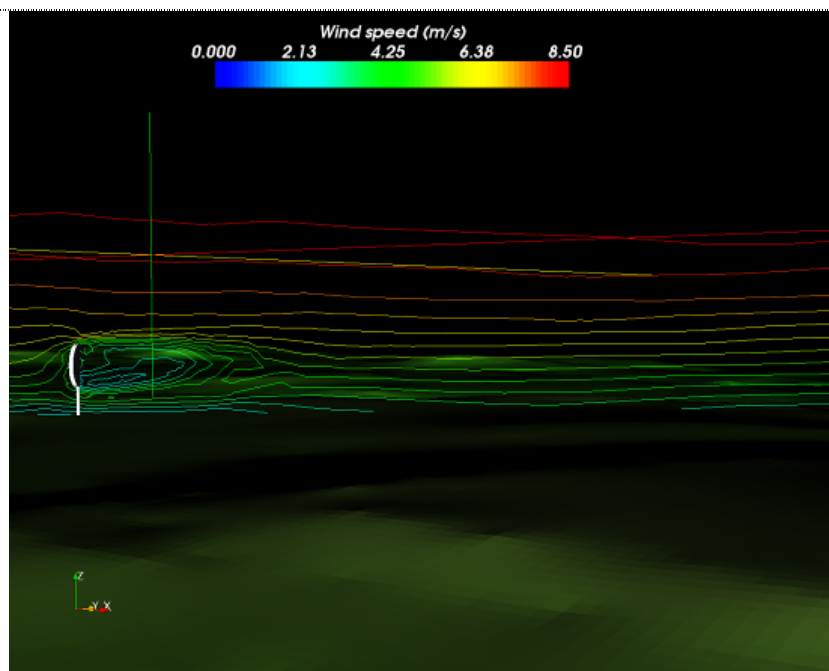
The wake is now fully developed. The grass drag has reduced the flow further near the ground (cyan strip).



### Contour plot at $t=900s$

The contour lines are plotted at intervals of 0.5 m/s. We can see that the wake is approximately 6-7 turbine diameters long.

Note the wake deficit is slightly greater nearer the ground: this is due to the strong vertical wind speed gradient.



### 3.5.3 Mesh evolution

As the simulation evolves, the computational complexity may increase or decrease due to the changing nature of the finite-element unstructured grid used by Fluidity. Fluidity uses an *hr*-adaptive algorithm to add elements to this grid where additional resolution, and remove them where the velocity gradients are shallow. It can also migrate mesh nodes with flow features.

Initially, the mesh is constructed with the largest elements far away from the turbine, getting progressively smaller towards the turbine, as demonstrated in Figure 22.

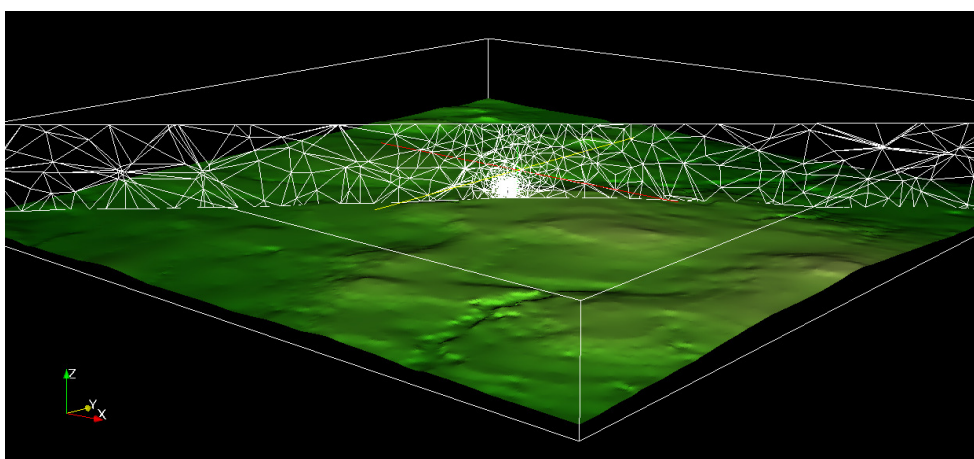


Figure 22: two-dimensional vertical slice through the mesh at  $t=0s$

However, this mesh will change as the simulation progresses, due to Fluidity's adaptive algorithms. In Figure 23, *hr*-adaptivity has increased the mesh resolution

overall, but particularly near the turbine – this is desirable, as it is near the turbine we require greater accuracy to model the wake.

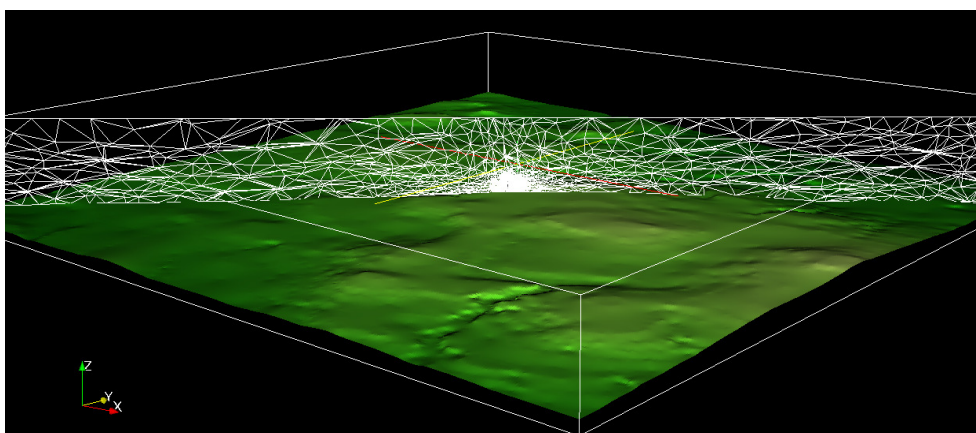


Figure 23: 3-dimensional vertical slice through the mesh at t=900s

The question is, then: how will the simulation scale over a long time, ie. will the resolution of the model increase to the extent that computational complexity overwhelms available processing power? To answer this, two simulation metrics were looked at:

- i) The size of the mesh data (VTU) files produced at each time-step , which give a measure of the computational complexity.
- ii) The time interval between each data dump, which is a measure of how long each time-step takes.

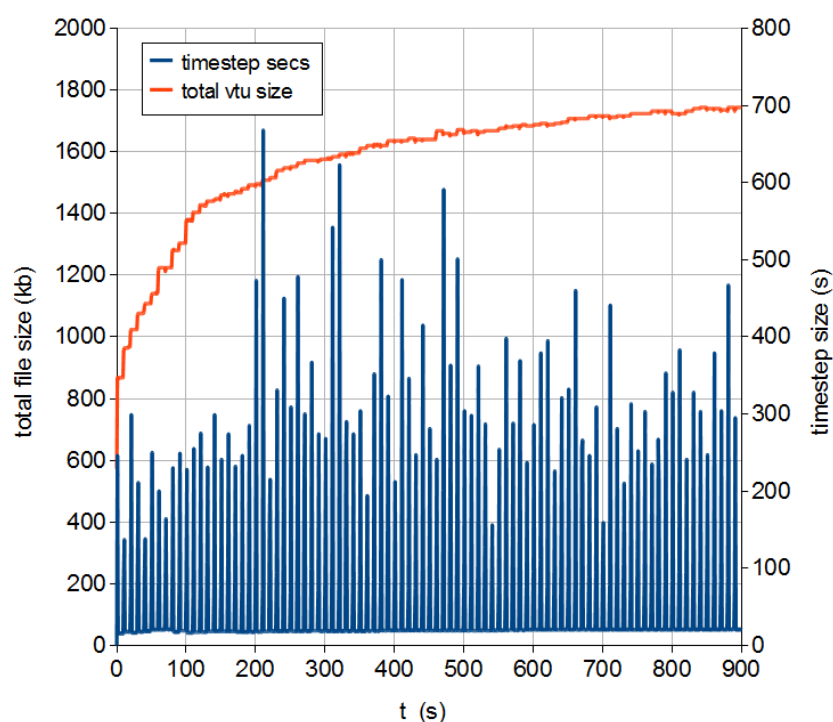
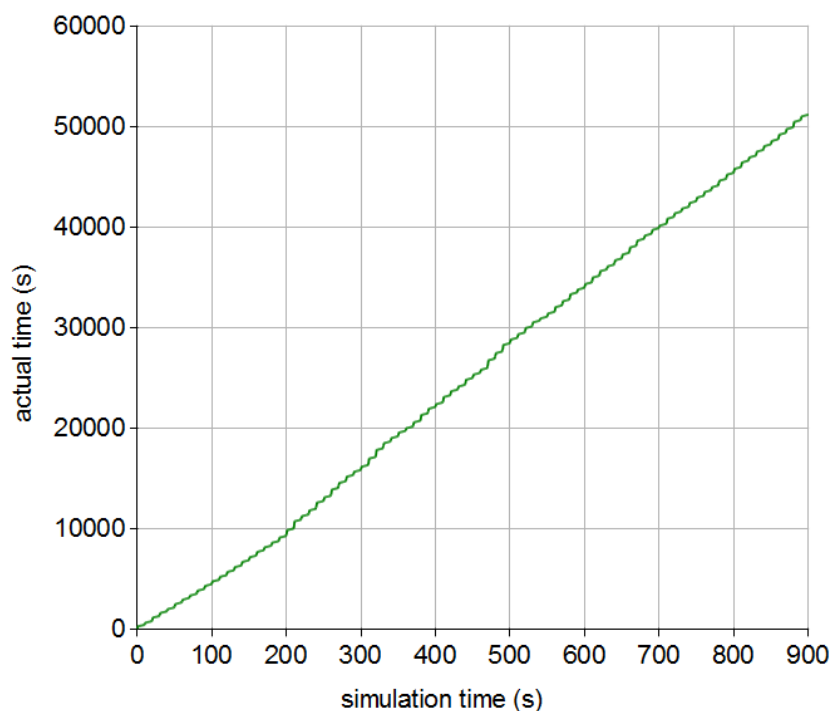


Figure 24: simulation time versus dump size and timestep size

Figure 24 shows us several things: firstly, that the data dump size has a near logarithmic shape, rapidly increasing at  $t < 150$ s, but levelling out towards the end of the simulation. Secondly, that whilst the period between simulation time-steps varies considerably near the start – this is due to large mesh adaptation steps taking variable amounts of time – towards the end, where the flow ‘settles down’, these vary less. Thirdly, it is clear that even though the size of the simulation may increase slightly, this does not adversely affect the running time.



**Figure 25: simulation time versus actual time passed**

Indeed Figure 25 confirms this last point: by plotting simulation time against the running time of the CFD program, we almost get a straight line. This strongly suggests that Fluidity, with appropriate adaptive algorithm parameters, will be well-behaved for large simulations of wind turbines or farms over long periods of time.

## 4 Discussion

The model represents a much greater level of detail of simulation than either WAsP or WindFarmer are capable of. In theory, this should either demonstrate or show the potential to demonstrate greater accuracy in simulation of air flow through modelled wind turbines, as well as surrounding environs including hills, gullies, trees, grass and water – or indeed any kind of terrain or ground features. In this section, we will examine aspects of the model and assess its effectiveness.

### 4.1 Qualitative assessment

#### 4.1.1 Turbine performance

The turbine clearly settles down in Figure 16 to a power output of just under 45kW. This is not the stated 105kW stated by the Danish Wind Association for this particular turbine<sup>11</sup>. However, looking at Figure 16 again, due to interference from ground objects, the conic shape of the LIDAR sweep, and the complex gradients therein – it is quite possible that 5 m/s may be a better estimate of hub-height free-stream velocity than 6 m/s. From the model contour plot (last slide in section 3.5.2), this would appear to be quite possible.

There are several points worth making here:

1. At a hub-height wind speed of 5 m/s, the Danish site has the Micon turbine producing 50kW of power – this puts the model within 14% of the official figures.
2. The skew between the turbine's orientation and the wind direction inevitably must lead to a drop in turbine performance. Therefore, we assume that performance of the model turbine is sub-optimal due to its skew of  $\sim 5^\circ$ .
3. Extrapolating (or more aptly, reverse engineering) the upwind boundary conditions from the limited LIDAR data given was a laborious task. With far-seeing LIDAR scans measuring upwind wind speeds, more accurate boundary conditions can be created.

(To this end, Sgurr have undertaken to produce more extensive LIDAR measurements – 3D sets of data, both upwind and downwind.)

Real validation can only come from comparison with actual turbine performance measurements. Unfortunately, as was previously stated access to these diagnostics is controlled by TUV NEL. Given scope and budget restrictions of this project (TUV NEL charge for this data), it was not possible to get this access. That said, steps are being taken to address this concern for future work, as will be detailed in section 5.

#### 4.1.2 Flow modelling over terrain

To make modelling over a 6km x 6km x 750m volume practical on a workstation, the minimum mesh resolution had to be low enough so that resources would be concentrated in modelling the turbine and its wake. That said, from looking at the large-scale vertical slices in section 3.5.2 and referencing them against Figure 6, we

can clearly see that the main causes of ground-based drag, the conifer plantations, have affected the flow both upwind and downwind.

What is not clear is how accurate this is, which raises two points:

1. Is the modelling of ground features such as trees as a quadratic-drag coefficient adequate? Sgurr's planned more extensive LIDAR measurements should verify this.
2. Trees actively produce turbulence, which may need to be factored in. One possible avenue is modelling the turbulence as a boundary condition through the Synthetic Eddy Method<sup>9</sup> – Fluidity is capable of doing this – which would require further LIDAR measurements from tree canopies so eddy length and frequency can be categorised.

Regarding topographic modelling, from the slides in section 3.5 we can clearly see the effect of ground based speed-up (or indeed slow-down, when going down hill), which shows the consequence of the Dirichlet condition  $\frac{\partial w}{\partial z} = 0$  on the ground, coupled with the continuity equation – an accelerative effect which competes with ground drag.

### 4.1.3 Wake modelling

Given the conical nature of the LIDAR sweep surface, it is extremely difficult to glean definitive answers, but it does appear from Figure 21 that the wake of the model is more extensive than that of the real turbine.

As turbulence acts as a catalyst for mixing between fluid layers, the *lack* of turbulence will result in a prolonged wake deficit which would have otherwise been dispersed by the entrainment of kinetic energy from the faster moving outer layers of the wake. This was the case in the model; turbulence was not generated at the boundaries, and so the ambient levels of turbulence would be lower within the simulation domain than the real site.

It was intended to incorporate turbulence measurements as boundary conditions through SEM, however difficulties in getting high-sample rate LIDAR data in time for this project meant this was not possible within the scope of the project.

## 4.2 Future work

As has been stated, Sgurr have agreed to provide further, extensive LIDAR measurements around the Micon turbine, both upwind and downwind, in successive slices so as to provide a fully three-dimensional set of data. This will allow much more detailed wake analysis than Figure 21 – ie. wake profile analysis in both radial and axial directions. This is an interim measure however, to future work being planned.

A research project is being proposed, to extend and validate the model in the following ways:

1. Incorporation of turbulence boundary conditions based upon LIDAR measurements\*.
2. Extensive validation with experimental measurement of a farm of micro-wind turbines.

3. Development of active pitch/turbine control system\*.
4. A concerted approach to building up a database of blade geometries etc. for popular commercial wind turbines – possibly contacting turbine manufacturers\*.
5. (*Long term goal*) The simulation of and comparison with full-size turbines, including performance data. Dr Creech has been in talks with a power company with access to a variety of wind farm sites and associated real-time turbine data.

This would be coupled with future research partnership with Sgurr, who through their Galion device would be able provide wake data for sites.

**\*Note:** these goals will require extra pairs of hands – HW may look into hiring additional help, ie. through PhD. studentships or hiring already established HW researchers for part-time assistance.

## 5 Conclusion

The Heriot-Watt turbine model has shown that it is possible to simulate unsteady air flow in a large simulation volume with irregular topography and ground features, as well as being able to resolve the finer details of the wake behind a wind turbine. It has also shown that it is possible to couple elements of Blade Element theory with computational fluid dynamics to produce a dynamic, reactive wind turbine model which produces similar performance and behaviour to that of a real turbine.

With the methodology developed to import terrain data and generate realistic wind profiles, in principle it has demonstrated that CFD methods have the potential to be a viable tool for wind farm analysis – with greater flexibility than analytic wake methods permit.